Tropical Sensitivity of a Coupled Model to Specified ISCCP Low Clouds

C. T. GORDON, A. ROSATI, AND R. GUDGEL

Geophysical Fluid Dynamics Laboratory, Princeton, New Jersey

(Manuscript received 28 April 1999, in final form 8 September 1999)

ABSTRACT

The seasonal cycle of SST observed in the eastern equatorial Pacific is poorly simulated by many ocean–atmosphere coupled GCMs. This deficiency may be partly due to an incorrect prediction of tropical marine stratocumulus (MSc). To explore this hypothesis, two basic multiyear simulations have been performed using a coupled GCM with seasonally varying solar radiation. The model's cloud prediction scheme, which underpredicts tropical marine stratocumulus, is used for all clouds in the control run. In contrast, in the ''ISCCP'' run, the climatological monthly mean low cloud fraction is specified over the open ocean, utilizing C2 data from the International Satellite Cloud Climatology Project (ISCCP). In this manner, the treatment of MSc clouds, including the annual cycle, is more realistic than in previous sensitivity studies.

Robust surface and subsurface thermodynamical and dynamical responses to the specified MSc are found in the Tropics, especially near the equator. In the annual mean, the equatorial cold tongue extends farther west and intensifies, while the east–west SST gradient is enhanced. A double SST maximum flanking the cold tongue becomes asymmetric about the equator. The SST annual cycle in the eastern equatorial Pacific strengthens, and the equatorial SST seasonal anomalies migrate farther westward. MSc-induced local shortwave radiative cooling enhances dynamical cooling associated with the southeast trades. The surface meridional wind stress in the extreme eastern equatorial Pacific remains southerly all year, while the surface zonal wind stress and equatorial upwelling intensify, as does the seasonal cycle of evaporation, in better agreement with observation. Within the ocean, the thermocline steepens and the Equatorial Undercurrent intensifies. When the low clouds are entirely removed, the SST warms by about 5.5 K in the western and central tropical Pacific, relative to ''ISCCP,'' and the model's SST bias there reverses sign.

ENSO-like interannual variability with a characteristic timescale of 3–5 yr is found in all simulations, though its amplitude varies. The ''ISCCP'' equatorial cold tongue inhibits the eastward progression of ENSO-like warm events east of the date line. When the specified low cloud fraction in ''ISCCP'' is reduced by 20%, the interannual variability amplifies somewhat and the coupled model responds more like a delayed oscillator. The apparent sensitivity in the equatorial Pacific to a 20% relative change in low cloud fraction may have some cautionary implications for seasonal prediction by coupled GCMs.

1. Introduction

The annual cycle in the eastern tropical Pacific has been a topic of considerable interest in recent years. Both components of the surface wind stress as well as the sea surface temperature (SST) exhibit a pronounced annual cycle in the eastern equatorial Pacific. Another prominent feature of the annual cycle, noted by Horel (1982) is the rapid phase propagation along the equator of SST and zonal wind seasonal anomalies. The climatological annual mean states of SST and the meridional components of the surface wind stress and ocean currents in the eastern tropical Pacific are asymmetric about the equator. There, colder SSTs are found south of the equator and warmer SSTs north of it, while the meridional components of the surface wind stress and ocean currents are directed northward at the equator year-round.

Observational studies such as Wallace et al. (1989), Mitchell and Wallace (1992), Wang (1994), and Nigam and Chao (1996) have shown the important role of air–sea interactions in the observed annual cycle. In the east, the ocean exhibits a dynamical response to the seasonal cycle of the surface winds. Eastward of longitude 100°W, the meridional component of surface wind stress induces coastal upwelling. The possibility of positive feedbacks also arises. Mitchell and Wallace proposed a positive feedback loop involving the meridional component of surface wind stress and SST. Along the equator, the annual cycle in surface wind stress affects equatorial upwelling.

Among the intriguing questions is: why there should be an annual cycle rather than a semiannual cycle on the equator, when the antisymmetric mode of solar radiative forcing is a minimum there? Also, why is the

Corresponding author address: Dr. C. T. Gordon, NOAA/GFDL, Princeton University, Forrestal Campus, US Route 1, P.O. Box 308, Princeton, NJ 08542.
E-mail: tg@gfdl.gov

annual cycle on the equator more in phase with the seasonal cycle in the Southern Hemisphere? Using the simple linearized coupled model approach, Xie (1996) discovered a westward propagating coupled instability mode that is antisymmetric about the equator. The instability is caused by a wind–evaporation–SST feedback. In the simple coupled model of Chang (1996), the air–sea interactions in the meridional direction are crucial to the development of the pronounced annual cycle in the near-coastal zone of the eastern tropical Pacific. In contrast, the air–sea interactions in the zonal direction are largely responsible for the westward expansion of the annual cycle along the equator.

The anomaly coupled model of Li and Philander (1996), with linearized dynamics, can maintain an annual cycle in the eastern tropical Pacific. Taking the asymmetric annual mean states there as given, the linearized meridional thermal advection term is antisymmetric about the equator. Thus, this term contributes to an annual cycle, whose amplitude will depend upon the amplitude of the air–sea interactions. Their model's SST annual cycle in the eastern equatorial Pacific was too weak, when evaporative flux alone was retained. Adding the upwelling term produced considerable amplification and a forward phase shift. The further addition of parameterized *marine stratocumulus* (often referred to hereinafter as MSc) clouds modestly enhanced the amplitude of the annual cycle, and slightly retarded its phase.

However, the linearized anomaly model approach begs the question of what sustains the asymmetric annual mean state. The fully nonlinear coupled ocean–atmosphere general circulation model (GCM) approach could conceivably provide more insight. Neelin et al. (1992) reviewed the status of coupled ocean–atmosphere models. Unfortunately, they found that the observed SST seasonal cycle and cold annual mean SSTs in the equatorial eastern Pacific were simulated quite poorly by many GCMs. In an updated review, Mechoso et al. (1995) reported some improvement. The deficiencies of many coupled GCMs, including the model of Rosati et al. (1997), may be due, in part, to their underprediction of subtropical MSc clouds (Browning 1994), and their inability to predict the *seasonal cycle* of those clouds. MSc respond directly to SST, atmospheric stability, and other factors as shown from the observational studies of Klein and Hartmann (1993) and others. In turn, MSc clouds have a direct local shortwave radiative cooling effect on SSTs, by reducing the net shortwave radiative flux at the surface. In a nonlinear coupled GCM, the possibility exists for positive feedbacks between MSc-induced shortwave radiative cooling and dynamical cooling mechanisms associated with the southeast trades. Conceivably, the strength of the annual cycle of SSTs in the tropical eastern Pacific could even have a nonlocal impact on other tropical phenomena, including the evolution of El Niño–Southern Oscillation (ENSO) events. Nigam (1997) has proposed a new feedback for the near coastal region of the eastern tropical Pacific from March until May, that is, longwave radiative cooling associated with MSc clouds generates southerly surface winds, which in turn foster the growth of MSc.

The approach of Li and Hogan (1999) is designed to side step the difficulties coupled GCMs may have maintaining the time mean state. Taking a cue from the findings of Li and Philander (1996), they nudged their own coupled GCM toward the observed time mean state, by imposing an annual mean flux adjustment. This type of flux adjustment may be less constraining than the seasonally varying type. In any case, their model responded by generating an improved seasonal cycle and robust interannual variability.

Three recent coupled GCM studies have explored the role of marine stratocumulus clouds in maintaining an asymmetric time mean state and the annual cycle. Philander et al. (1996) considered various mechanisms, including the impact of empirically predicted MSc cloud fraction upon the dynamics that might explain why the ITCZ is mostly north of the equator. The MSc cloud fraction served as an input parameter of an empirical, surface shortwave radiative flux correction for the ocean, but did not directly affect the atmospheric radiation. Whereas all else failed, their MSc clouds amplified preexisting weak asymmetries, to generate an asymmetric SST distribution about the equator in the eastern tropical Pacific. In their view, this seems to be a prerequisite for successfully simulating the annual cycle in the eastern tropical Pacific. However, they could not specifically address the seasonal cycle, since annual mean solar radiation was employed.

Ma et al. (1996) specified idealized marine stratocumulus with a cloud fraction of 100% year-round off the coast of Peru and studied its impact upon SST in the eastern tropical Pacific. Their idealized Peruvian MSc reduced the warm SST bias in the southeastern tropical Pacific of their GCM. Yu and Mechoso (1999) have examined the impact of seasonally varying Peruvian MSc by specifying MSc either during the first half or during the second half of the year. The latter, more realistic seasonal variation of the MSc clouds appeared to be crucial for simulating the seasonal cycles of SST and dynamical and evaporative cooling in the eastern tropical Pacific.

In this study, we examine the tropical response of our coupled GCM to quasi-realistic *specified* MSc (and other low) clouds versus those currently predicted by our coupled GCM. Our strategy was guided by the following considerations. Although the complex physical processes affecting MSc have become somewhat better understood since the survey by Browning (1994), most MSc schemes, including our own, used in current coupled GCMs still inadequately predict MSc cloud fraction and cloud optical properties. The deficiencies include the lack of prognostic cloud water (in some GCMs), insufficiently detailed microphysical processes such as

drizzle formation, and incomplete representation of mixing processes across the inversion and of exchanges of heat and moisture between the surface and the boundary layer. Second, other biases of a coupled GCM could adversely affect the performance of the perfect scheme for predicting MSc. On the other hand, analyses of cloud, derived from satellite measurements of radiation at the top of the atmosphere, are now available.

As in Yu and Mechoso (1999), the role of MSc in maintaining the annual cycle in the eastern tropical Pacific and the mechanisms involved will be addressed. A robust equatorial dynamical response to MSc forcing is a significant finding. However, our approach is novel in several aspects. First, a *seasonally varying* low cloud fraction field is specified over the open ocean, utilizing monthly mean low cloud data from the International Satellite Cloud Climatology Project (ISCCP). With *seasonally varying* ISCCP cloud data, the SST response and its causes may be explored in a more realistic setting than has been done heretofore. Second, integrating a different model for a longer period, that is, 23 yr, offers some check on the robustness of results of earlier, more idealized studies. Third, an auxiliary experiment without low clouds helps to clarify the impacts of low clouds on the tropical thermodynamical and dynamical responses. Fourth, the interannual SST response is examined. Fifth, the sensitivity of the SST interannual response to relatively small fluctuations in specified low cloud fraction is analyzed. The latter two aspects are both of potential interest to the ENSO prediction problem.

The coupled model is briefly described in section 2. The experimental design of the basic and auxiliary integrations, the initial conditions and verification datasets are mentioned in section 3. The annual mean and seasonal cycle equatorial responses from the multiyear simulations are examined in section 4. The interannual variability responses are described in section 5. Equatorial cold tongue dynamics is discussed in section 6. Concluding remarks are presented in section 7.

2. Description of the coupled model

The Modular Ocean Model (MOM) (Pacanowski 1995) has been coupled to a global atmospheric GCM. The MOM (version 1) has 1° horizontal resolution (except for ⅓° in the meridional direction between latitudes 10°N and 10°S) on a staggered B grid, 15 vertical levels, and static stability-dependent vertical mixing based upon a Mellor and Yamada level 2.5 turbulence closure scheme. The configuration of the MOM employed in the present investigation and its coupling to the atmospheric GCM are described in Rosati et al. (1997).

The atmospheric GCM has evolved from the Gordon and Stern (1982) global spectral model. The version employed here has T30 (triangular 30) spectral horizontal resolution, 18 sigma levels in the vertical, and Gibbs-filtered orography. It incorporates most of the physical parameterizations found in Stern and Miyakoda (1995), although a few have been modified, replaced, or switched off. Among those retained intact are: static stability-dependent vertical mixing, based upon a Monin–Obukhov formulation in the surface layer, and a Mellor and Yamada level 2.5 turbulence closure scheme in the planetary boundary layer and free atmosphere; water bucket hydrology; and gravity wave drag.

Full radiation is calculated every 12 h, and the solar radiation is seasonally varying but not diurnally varying. The radiative transfer algorithms are essentially the same as documented in Gordon (1992). However, instead of being a constant, that is, 0.9942, the near-infrared single-scattering albedo, $\omega_{o,ir}$, is now a piecewise continuous, monotonic function of zonal mean saturation water vapor mixing ratio, $\langle q_s \rangle$, at the bottom sigma level (level 18). Here $\omega_{o,ir}$ attains its maximum value, 0.970, for $\langle q_s \rangle \geq 2.0 \times 10^{-2}$. Cloud absorption is moderately enhanced in the Tropics by this parameterization. The physical basis for anomalous cloud absorption is controversial. Observational evidence in support of it, cited by Cess et al. (1994) has been questioned by others. Originally, it was implemented in our atmosphere-only model to control its tropical zonal mean net absorbed shortwave bias. In the coupled model version, the SST cold bias in the western tropical Pacific decreases by ~0.5°C.

The most drastic modification is that the Arakawa–Schubert (AS) parameterization of cumulus convection (Sirutis and Miyakoda 1990) has replaced the moist convective adjustment (MCA) scheme. With AS cumulus convection, model-simulated SSTs are generally >2°C warmer over the Pacific basin (Sirutis and Rosati 1996).

The diagnostic cloud prediction scheme of Gordon (1992) was retuned for AS convection to counteract the effect of its moister atmosphere upon the scheme. Namely, the threshold relative humidity for stratiform clouds was raised from 70% to 80% and the linear relationship between cloud fraction and relative humidity was replaced by a quadratic one. Even so, the upper troposphere is more cloudy with AS than with MCA.

The algorithm for MSc cloud fraction has also been revised, in an attempt to improve the simulation of tropical MSc. In Gordon (1992), MSc low cloud fraction was diagnosed as a linear function of dry static stability of the most stably stratified model layer in the lower troposphere, with relative humidity as an auxiliary predictor, based upon a relationship developed by Slingo (1987) for the European Centre for Medium-Range Weather Forecasts model. The revised scheme utilizes an approach similar to Philander et al. (1996), whereby the temperature difference between 850 hPa and the surface is the sole predictor, and ISCCP cloud data is used to derive the linear regression formula. Unfortunately, when employed in our *coupled model* integrations, it quickly becomes ineffective, as the developing warm SST bias in the MSc region is associated with a concurrent reduction in lower-tropospheric static sta-

bility there. Constant values of cloud optical depth for low, middle, high (anvil cirrus), and convective clouds, that is, $\tau_1 = 9.0$, $\tau_m = 6.0$, $\tau_h = 2.5$, and $\tau_{\text{cnv}} = 18.0$, are used to calculate cloud emissivity, reflectance and absorptance, in all integrations, as in Gordon (1992). Also, all high clouds are assumed to be anvil cirrus (with emissivity close to 1).

3. Experimental setup

The basic experiment consists of a pair of integrations, which differ only in the treatment of low cloud fraction over the open ocean. It is predicted in the control integration (hereinafter CNTRL), whereas a 1984–90 "climatology" of monthly mean low cloud fraction, derived from ISCCP C2 monthly diurnal mean data (Rossow and Schiffer 1991), is linearly time interpolated to radiation time steps for insertion into the model in the ISCCP integration (hereinafter ''ISCCP''). The monthly diurnal mean low cloud fraction is actually computed as

$$\text{low} = \text{total} - \text{high} - \text{middle}, \quad (1)$$

where total, high, and middle denote the ISCCP C2 monthly diurnal mean total, high, and middle cloud fractions, respectively. This formula is preferable to using ISCCP C2 low cloud fraction data directly, because shortwave radiances are a better discriminator than infrared radiances of marine stratocumulus clouds. However, in the ISCCP C2 dataset, only the total cloud fraction is derived from both shortwave and infrared radiances; its low, middle, and high cloud fractions are all derived from infrared radiances only. Equation (1) is consistent with the overlap assumptions used to generate the ISCCP C2 IR-marginal total cloud amount. ISCCP cloud-top pressure data are employed to position the ISCCP low clouds within the vertical column. In the present suite of experiments, those clouds are assumed to be one sigma layer thick, being centered at full sigma levels. In all runs, low cloud fraction is still predicted over land and sea ice, while middle and high cloud fractions are predicted everywhere. Predicted low clouds are usually one, but sometimes two, sigma layers thick.

The above approach captures the essence of the ''sensitivity of the seasonal cycle to marine stratocumulus'' problem, since the ISCCP low cloud classification applies mainly to boundary layer clouds, including MSc. (In contrast, clouds associated with synoptic systems having higher tops, would tend to be categorized in ISCCP C2 as middle clouds.) By predicting middle and high cloud fractions, the constraint that specified climatological mean low cloud fraction might impose on equatorial interannual variability is relaxed somewhat. Also, the sensitivity of the simulated outgoing longwave radiation budget to clouds (which is strongest for high clouds) may be reduced. Retaining the predicted low cloud fraction over land should temper cloud-induced differences in the ''ISCCP'' versus CNTRL land surface heat budgets, since there is relatively little low cloudiness over land according to ISCCP. Otherwise, such differences could potentially affect the general circulation and the oceanic response. Specification of the same fixed cloud optical depths in both the CNTRL and ''ISCCP'' experiments simplifies the analysis of the results.

TABLE 1. Treatment of low clouds in various simulation experiments.

Experiment	Low cloud fraction over the open ocean
CNTRL	Fully predicted by diagnostic cloud scheme.
''ISCCP''	Specified from the ISCCP C2, seasonally varying 1984–90 7-yr climatology.
ISC.8	Same as ''ISCCP,'' except the ISCCP low cloud fraction is scaled by 0.8.
NOLOW	Set low cloud fraction = 0, over the open ocean.
HYB	Hybrid of ''ISCCP'' in the eastern tropical Pacific (120–65°W, 30°S–20°N) and CNTRL elsewhere.

Some auxiliary multiyear simulation experiments have also been performed. In NOLOW, the predicted low cloud fraction is reset to zero over the entire open world ocean, including over the MSc regions, but is retained over land and sea ice. This highly idealized experiment provides some insight into the coupled model's ''ISCCP'' minus CNTRL dynamical response to MSc forcing. Additionally, comparison of the ''ISCCP'' versus NOLOW SST biases in the western equatorial Pacific suggests how sensitive our current coupled system is to biases in (low) cloud-radiative forcing there. HYB is a hybrid of NOLOW and ''ISCCP.'' Here, predicted low cloud amount is reset to zero over the entire open World Ocean, except in the eastern tropical Pacific domain (120°–65°W and 30°S–20°N), where ISCCP low cloud amount is specified. HYB results will confirm whether the impact of ISCCP clouds in the eastern tropical Pacific remains qualitatively intact, when the low cloud fraction farther west decreases substantially. The ISCCP low cloud amount field is scaled by 0.8 in ISC.8, to test the sensitivity of the interannual variability response to a relatively modest change in MSc cloud fraction. Salient characteristics of the low clouds in CNTRL, ''ISCCP,'' and auxiliary experiments are summarized in Table 1.

All multiyear integrations were started from 1 January 1982 initial conditions. The atmospheric initial conditions were obtained from the National Centers for Environmental Prediction, while the oceanic initial conditions were generated by the four dimensional ocean data assimilation (ODA) system of Rosati et al. (1995).

The CNTRL, ''ISCCP,'' ISC.8, NOLOW, and HYB simulations were all integrated for 23 yr. The first 3 yr of integration have been excluded from the calculated climatologies due to significant model drifts in SST in the tropical Pacific basin. The ''ISCCP'' simulation cooled in the western equatorial Pacific while the seasonal cycle intensified in the east. CNTRL adjusted in

the eastern tropical Pacific ~1 yr sooner than ''ISCCP.'' Perhaps the model's preferred state was closer to the initial conditions. A warming trend in SST persisted considerably longer in NOLOW and HYB.

We rely mainly on the Comprehensive Ocean–Atmosphere Data Set (COADS) analysis of da Silva et al. (1994), for verifying SSTs and surface wind stress. The Global Sea-Ice and Sea Surface Temperature (GISST2) analysis (Rayner et al. 1996) is also used. Top of the atmosphere (TOA) radiative fluxes are verified against Earth Radiation Budget Experiment (ERBE) narrow field of view radiative fluxes (Barkstrom et al. 1990). Surface flux components are verified against the COADS analysis (da Silva et al. 1994) and the Pinker and Laszlo (1992) satellite-dependent analysis of surface shortwave flux. All model-simulated and verification TOA and surface data, including SST, are sampled on the atmospheric spectral model's T30 (96×48) transform grid. Ocean temperatures are verified against the Levitus (1982) climatological atlas and the ODA.

4. Multiyear simulations: Annual mean and seasonal cycle results

a. Clouds and radiation

In July, the largest differences in ''ISCCP'' versus CNTRL low cloud fraction (Fig. 1) are found in the southeastern tropical Pacific. As anticipated, the CNTRL simulation drastically underpredicts the prominent observed MSc feature off the coast of Peru. On the other hand, the model's cloud prediction scheme manages to capture some of the low cloud off the coast of California. This contrasting behavior of the two regions is related to SST drift, which occurs in the coupled model simulation. As noted by Philander et al. (1996), seasonal variations in dry static stability are controlled mainly by variations in SST in the eastern tropical Pacific. Hence, as a warm SST bias develops in the eastern tropical Pacific, the dry static stability in the lower troposphere decreases. In turn, less low cloud is predicted by the linear regression relationship between model static stability and observed low cloud fraction. Conversely, variations in tropospheric temperature (e.g., at 850 hPa) play a greater role in the extratropics, thereby enabling some low cloud off the coast of California to survive.

The ''ISCCP'' low cloud fraction exhibits a very strong annual cycle in the southeastern tropical Pacific. At longitude 94°W (Fig. 2), it achieves its maximum value (>0.8) during late August, at latitude 9°S or 10°S. A secondary maximum is found north of the equator, near 2°N, approximately 2 months later. The minimum value is found in March between the equator and latitude 10°S. North of the equator, there is much less low cloud and perhaps a weak semiannual cycle in ''ISCCP.'' In contrast, CNTRL exhibits an erroneous annual cycle in the Northern Hemisphere.

Interannual variations in monthly mean low cloud fraction to the west of Peru (not shown) as large as O(0.2) were found in the ISCCP C2 dataset. While such interannual variability does not stand out compared to that in observed low or high cloud fraction elsewhere in the Tropics, it could nonetheless modulate ENSO warm and cold events.

The impact of low cloud fraction on shortwave radiative fluxes represents the primary forcing in the current sensitivity study. Although the surface shortwave radiative flux directly affects the tropical ocean, the TOA net absorbed shortwave (incident solar minus reflected solar) flux is more reliably observed. Moreover, these two variables are interrelated. Time series of monthly mean TOA net absorbed shortwave flux in Niño-1+2, (90°–80°W, 10°S–0°), are plotted in Fig. 3, for the CNTRL simulation, the ''ISCCP'' simulation (with *climatological* monthly mean ISCCP C2 low clouds), and ERBE. Niño-1+2 is imbedded in the MSc region of the southeastern tropical Pacific. The phase and dominance of the annual harmonic in the seasonal cycle is considerably more accurate in ''ISCCP'' than in CNTRL. Clearly, realistic specification of low cloud fraction in the MSc region has a favorable impact on the local TOA shortwave balance. Weak interannual variability in ''ISCCP'' is probably attributable to the predicted middle and high clouds. With interannually varying ISCCP low clouds, ''ISCCP'' and ERBE should agree even more closely. Assuming that the ISCCP low cloud fraction is realistic, the results of Fig. 3 suggest that our specified cloud optical depth is fairly reasonable in the MSc region too.

''ISCCP'' and CNTRL surface net shortwave radiative flux fields are verified against the COADS analysis in July (Fig. 4). These surface flux components tend to be somewhat larger than the opposing longwave surface fluxes. In the southeastern tropical Pacific, ''ISCCP'' bears noticeably closer resemblance, overall, to both COADS and the Pinker and Laszlo (1992) analysis (not shown) than CNTRL does, especially in summer and autumn, when the ''ISCCP'' minus CNTRL MSc cloud forcing is strongest. In contrast, in other regions, for example, in the central tropical Pacific, where the low cloud forcing is weaker, both ''ISCCP'' and CNTRL appear to verify poorly against COADS. Even so, the apparent negative biases in simulated shortwave radiative flux in the western tropical Pacific are probably real. Also, the SST there may be locally quite sensitive to those biases.

b. The tropical SST and surface wind stress responses

Contour maps of climatological annual mean SST over the tropical Pacific basin are displayed in Fig. 5 for ''ISCCP,'' CNTRL, and COADS. The 20-yr (1985–2004) and 40-yr (1950–89) climatologies are employed for the simulations and for COADS, respectively. Surface wind stress arrows are superposed.

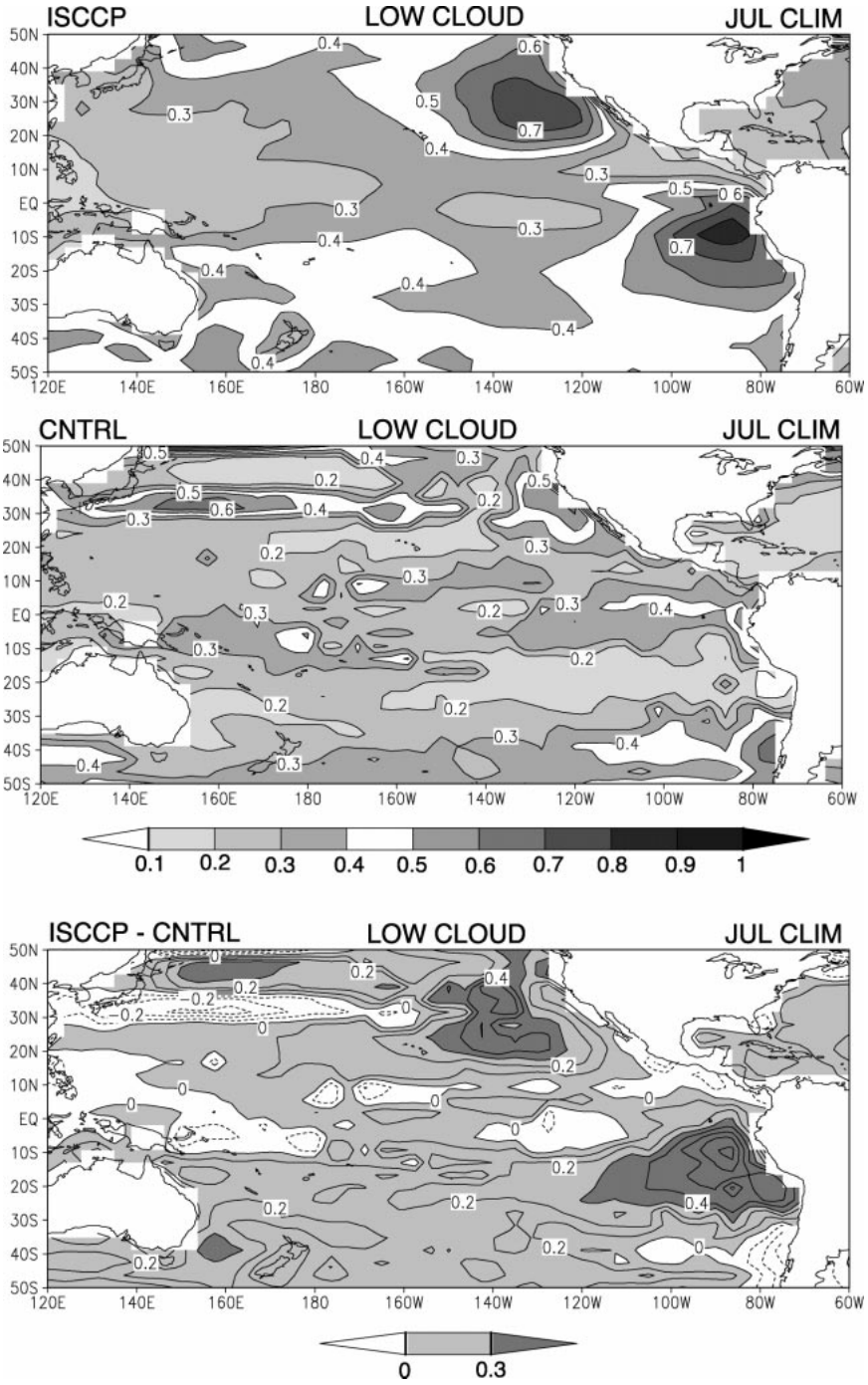

FIG. 1. Contour maps (120°E–60°W, 50°S–50°N) of 20-yr (1985–2004) Jul climatological monthly mean low cloud fraction. (top) ''ISCCP,'' (middle) CNTRL, and (bottom) ''ISCCP'' minus CNTRL difference field. Top and middle panels: shading is progressive, except none for (0.4, 0.5). Bottom panel: no shading (<0), light shading (0, 0.3), and darker shading (>0.3). Contour interval = 0.1. Negative contours are dashed. Continents are masked (no shading).

In the eastern equatorial Pacific, SSTs are nearly 2°C colder in ''ISCCP'' than in CNTRL and, in fact, are colder than observed. Furthermore, the annual mean east–west SST gradient in the eastern equatorial Pacific (Fig. 5) is much more pronounced in ''ISCCP'' than in CNTRL. The equatorial cold tongue is stronger and extends farther westward in ''ISCCP.'' In the annual mean, both simulations display a double SST maximum flanking both sides of the equatorial cold tongue. However, in ''ISCCP,'' the southern SST maximum does not pro-

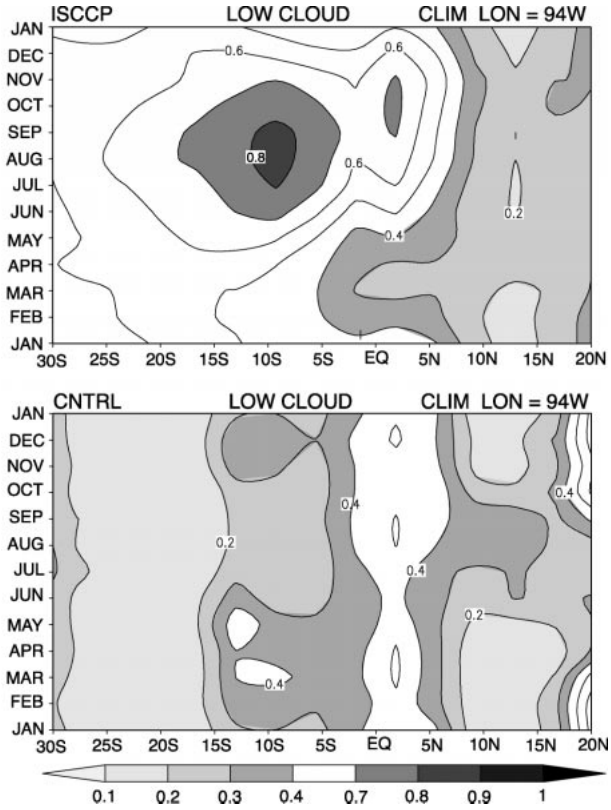

FIG. 2. Time–latitude sections of 10-yr (1985–94) climatological monthly mean low cloud fraction over one seasonal cycle at longitude 94°W. Latitude range = 30°S–20°N. (top) ''ISCCP'' and (bottom) CNTRL. Progressively darker shading with increasing cloud fraction, except none from 0.4 to 0.7. Contour interval = 0.1.

trude as far east as the northern SST maximum, in somewhat better agreement with COADS. Seasonally, the latitudinal asymmetry is strongest during boreal summer and early autumn. The corresponding simulated tropical precipitation patterns (not shown) exhibit similarly shaped patterns. In NOLOW (not shown), the cold tongue is barely discernible. Thus, it appears that the equatorial cold tongue and latitudinally asymmetric SST patterns flanking it is not well sustained without realistic tropical MSc.

Another striking feature of Fig. 5 are the *cold* biases in the western tropical Pacific. They are of the order of 1.5° and 2.5°C, respectively, in CNTRL and ''ISCCP.'' These cold biases suggest that our shortwave cloud forcing is too strong in the western tropical Pacific. Indeed, ISCCP data indicate that our global constant value of low cloud optical depth ($\tau = 9$) is too large for this region, although fairly reasonable for the MSc region. In contrast, NOLOW (not shown) exhibits a *warm* bias of nearly 3°C. Lacking any MSc clouds, its warm pool extends eastward across the Pacific, and its cold tongue is exceptionally weak. Most of the ~5.5°C SST warming in the western tropical Pacific between ''ISCCP'' and NOLOW is associated with the local reduction in low cloud fraction there from ~25%–30% in ''ISCCP'' to 0% in NOLOW and corresponding ~66 W m^{-2} increase in surface net shortwave radiation. This change implies an apparent local sensitivity of ~1°C (11 W m^{-2})$^{-1}$ (with other variables free to vary). However, ~1°C of the warming represents a remote response to the reduction in low cloud fraction farther east.

Although NOLOW has weaker annual mean equatorial zonal SST gradients (as well as weaker surface easterlies) than CNTRL, they do not entirely vanish. Seager and Murtugudde (1997) have shown that a zonal SST gradient can survive even in the presence of uniform surface heating. The latter is not imposed over the equatorial Pacific in any of the above experiments. However, in NOLOW, the surface net shortwave radiative flux is quite spatially uniform over much of the equatorial Pacific. This is not surprising considering that its low cloud amount is zero, the cloud optical depths are constants, and shortwave heating in our model is dominated by low clouds.

Not all of the SST response in the eastern equatorial

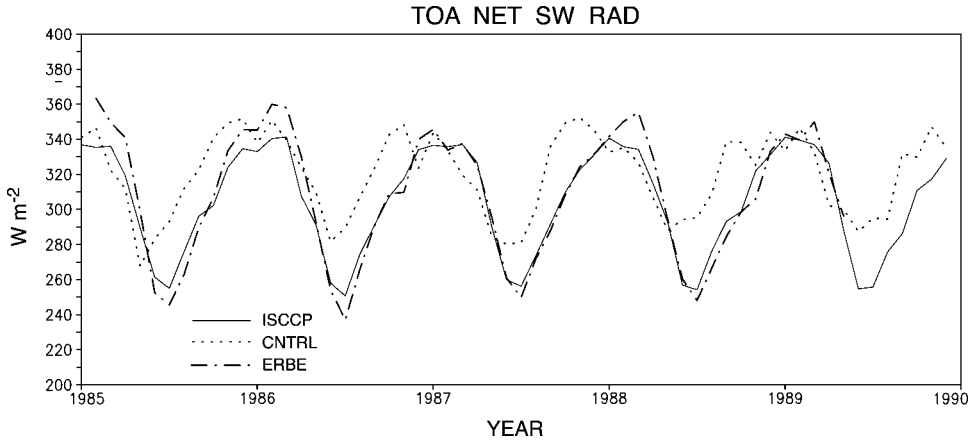

FIG. 3. Time series of monthly mean Niño-1+2 (90°–80°W, 10°S–0°) CNTRL, ''ISCCP,'' and ERBE TOA net absorbed shortwave radiative flux (W m^{-2}).

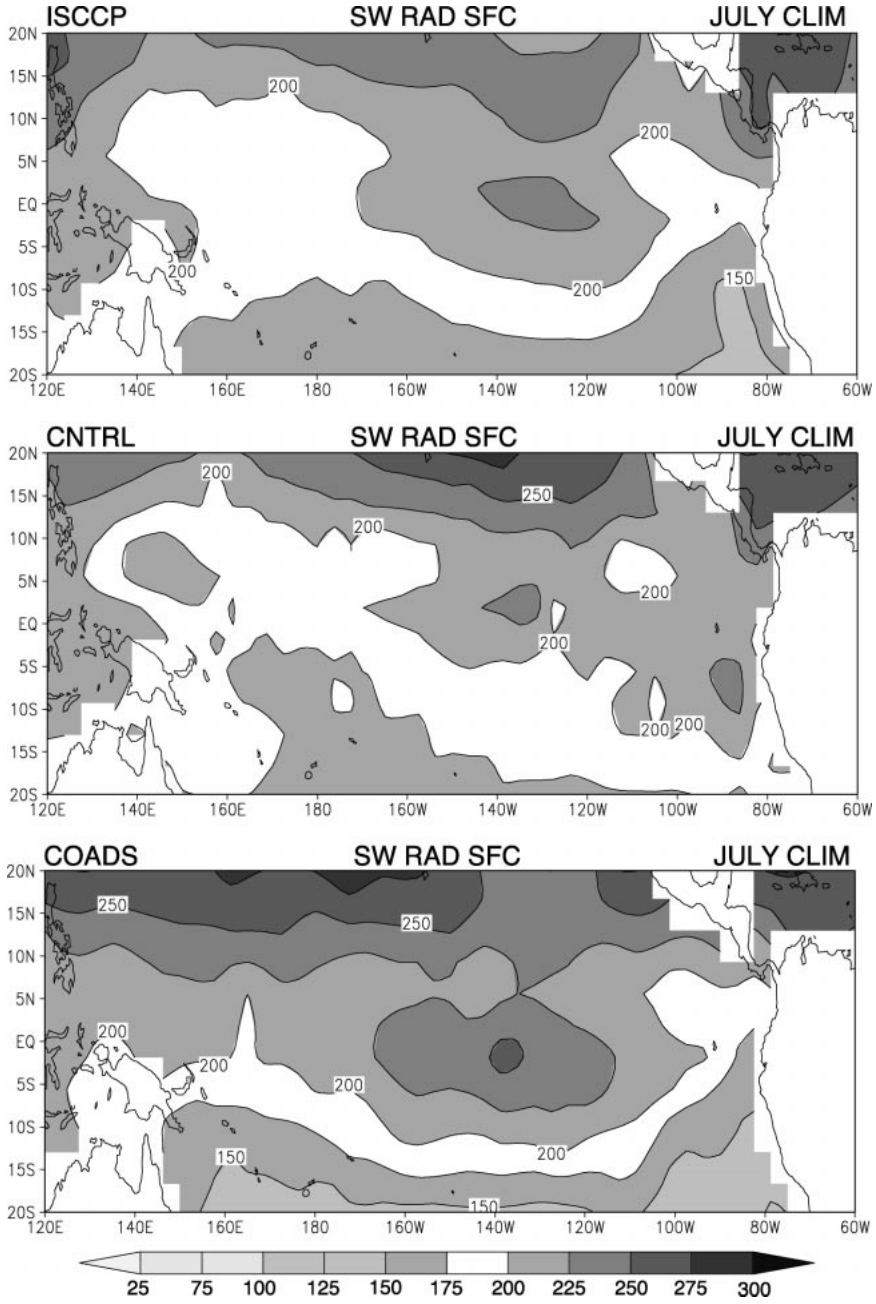

FIG. 4. Contour maps (120°E–60°W, 20°S–20°N) of Jul monthly mean surface net shortwave radiative flux. (top) ''ISCCP'' and (middle) CNTRL 20-yr climatologies. (bottom) COADS 8-yr (1982–89) climatology. Contour interval = 25 W m^{-2}. Progressively darker shading with increasing flux, except none from 175 to 200 W m^{-2}. Continents are masked (no shading).

Pacific (and even farther west) to changes in low cloud amount is due to direct radiative effects. In fact, evidence, including the wind stress vectors in Fig. 5 (discussed later), suggests that more MSc cloudiness in the eastern tropical Pacific induces stronger trades, and hence increased dynamical cooling through more intense upwelling, as well as a stronger annual cycle of evaporation. The enhanced equatorial upwelling extends across much of the equatorial Pacific, even west of the date line, where the ''ISCCP'' minus CNTRL differential low cloud forcing is much weaker than in the southeastern tropical Pacific. Some hint of this dynamical cooling response may be inferred from Fig. 5, where the annual mean equatorial SST is ~1°C colder in ''ISCCP'' than in CNTRL, west of the date line. In contrast, in NOLOW, greater net longwave and evap-

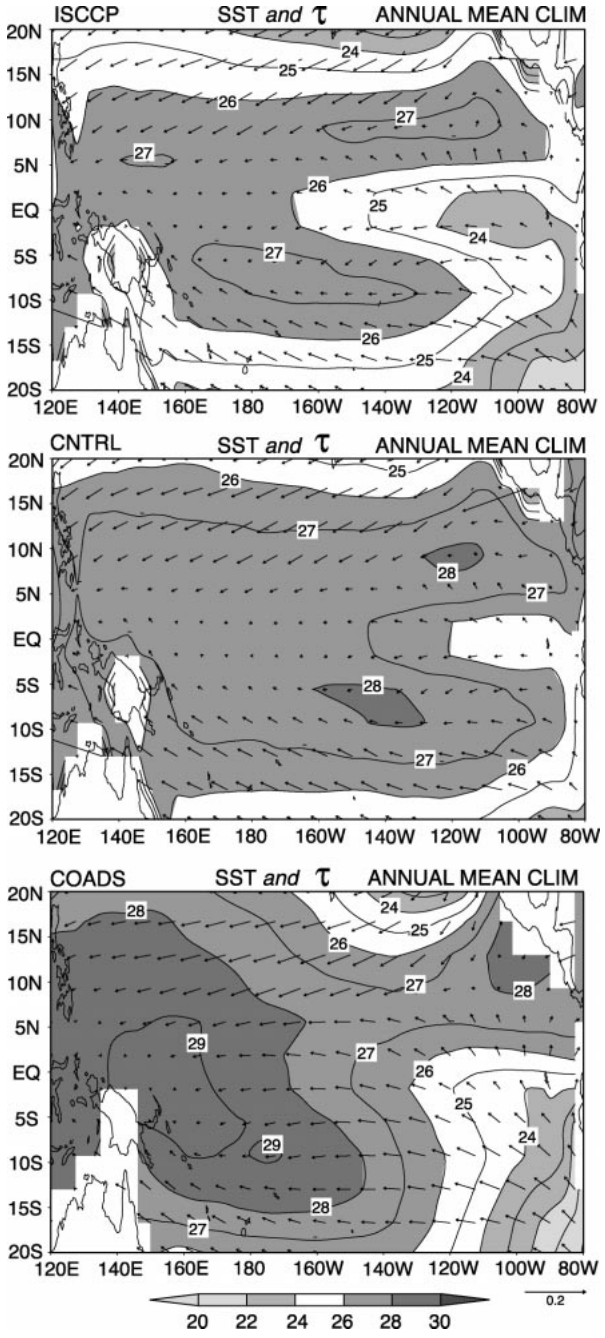

FIG. 5. Contour maps (120°E–80°W, 20°S–20°N) of annual mean SST with surface wind stress arrows superimposed. (top) ''ISCCP'' and (middle) CNTRL 20-yr (1985–2004) climatologies. (bottom) COADS 40-yr (1950–89) climatology. SST contour interval = 1°C. Progressively darker shading from colder to warmer values, except none from 24° to 26°C. Arrow length ∝ to wind stress magnitude, normalized by 0.2 Pa (near ''color'' bar). Land is masked (no shading).

orative fluxes oppose the increase in net shortwave radiation at the surface.

Seasonal SST anomalies (Figs. 6a and 6b) reverse sign between spring and autumn in both simulations, Yet, they are somewhat more realistic in ''ISCCP'' than in CNTRL. For example, in the southeastern tropical Pacific, the ''ISCCP'' anomalies are stronger, (though they are weaker and located farther off the coast compared to COADS). Also, the ''ISCCP'' warm anomalies (in spring) and cold anomalies (in autumn) extend farther north, cross the equator, and develop more pronounced equatorial tongues.

Horel (1982) showed that the westward migration of SST anomalies is a prominent feature of the annual cycle in the eastern equatorial Pacific. CNTRL manages to exhibit an annual cycle in SST (Fig. 7) in the eastern equatorial Pacific, despite its poor simulation of MSc off the coast of Peru. However, its annual cycle is confined essentially east of longitude 100°W. In contrast, the seasonal migration of ''ISCCP'' SST anomalies extends much farther westward, in better agreement with observation. Curiously, in a *linearized* anomaly model run of Li and Philander (1996), with MSc clouds, but no nonlinear cloud–dynamical interactions, the westward phase propagation of SST anomalies was quite weak, although the SST anomalies were quite strong. With no low clouds over the ocean, the NOLOW SST seasonal cycle (not shown) is essentially zonally symmetric across the equatorial Pacific and lacks any annual component in the east. A deficiency common to both the ''ISCCP'' and CNTRL simulations is that the maximum cold anomaly centered near longitude 90°W occurs approximately 6 weeks too early.

The annual mean tropical surface wind stress response may be deduced from the surface wind stress vectors in Fig. 5, which overlay the annual mean SST contours. In the southeastern tropical Pacific, east of 120°W, the ''ISCCP'' annual mean surface wind stress verifies better than CNTRL, by virtue of its greater amplitude and more northerly orientation. Similarly, in the eastern equatorial Pacific, the orientation and strength of the ''ISCCP'' cross-equatorial surface wind stress verify slightly better. Moreover, ''ISCCP'' should exhibit stronger south-to-north countergradient SST advection just north of the equator than CNTRL. Farther north, the surface convergence, which may feed the convection straddling the west coast of Central America, is stronger in ''ISCCP.'' Also, stronger easterly surface wind stress and stronger surface divergence (which favors enhanced equatorial upwelling) prevail in ''ISCCP,'' near the equator, east of the date line, in better agreement with COADS. On the other hand, the easterly component of surface wind stress is too weak west of the date line in both simulations.

c. SST, surface heat flux, and surface wind stress responses in Niño-3

Is the ''ISCCP'' minus CNTRL SST annual cycle response in the eastern equatorial Pacific essentially a direct, local radiative response, or does a significant, nonlocal positive cloud–dynamical coupled model response occur? To help to answer this fundamental ques-

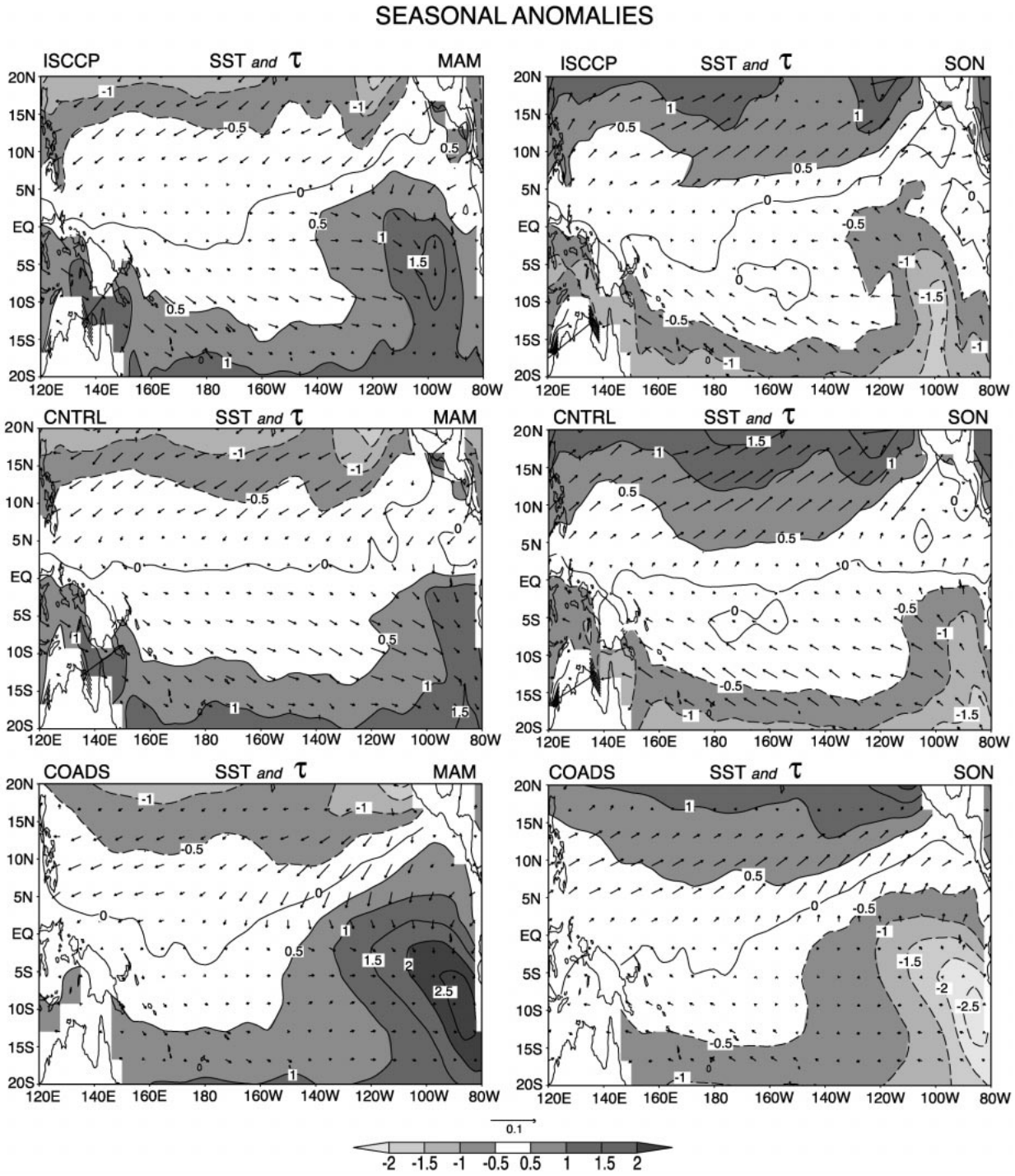

FIG. 6. Seasonal mean SST and surface wind stress anomalies relative to their annual mean climatologies in Fig. 5. SST contour interval = 0.5°C. Progressively darker shading from colder to warmer values, except none for −0.5° to 0.5°C. Anomaly wind stress arrows normalized by 0.1 Pa. (left) Spring (Mar–May) and (right) autumn (Sep–Nov).

tion, we examine the climatological mean seasonal cycles of selected near-surface variables in Niño-3 (150°–90°W, 5°S–5°N), a quintessential region for ENSO prediction. Note that it lies outside of the primary MSc cloud-forcing region.

Clearly, from Fig. 8, ''ISCCP'' simulates the Niño-3 SST seasonal cycle the best. Although its annual mean SST is ~1.5°C too cold, its annual harmonic dominates, with quite realistic amplitude and phase. In contrast, the CNTRL annual cycle is much weaker, and exhibits a

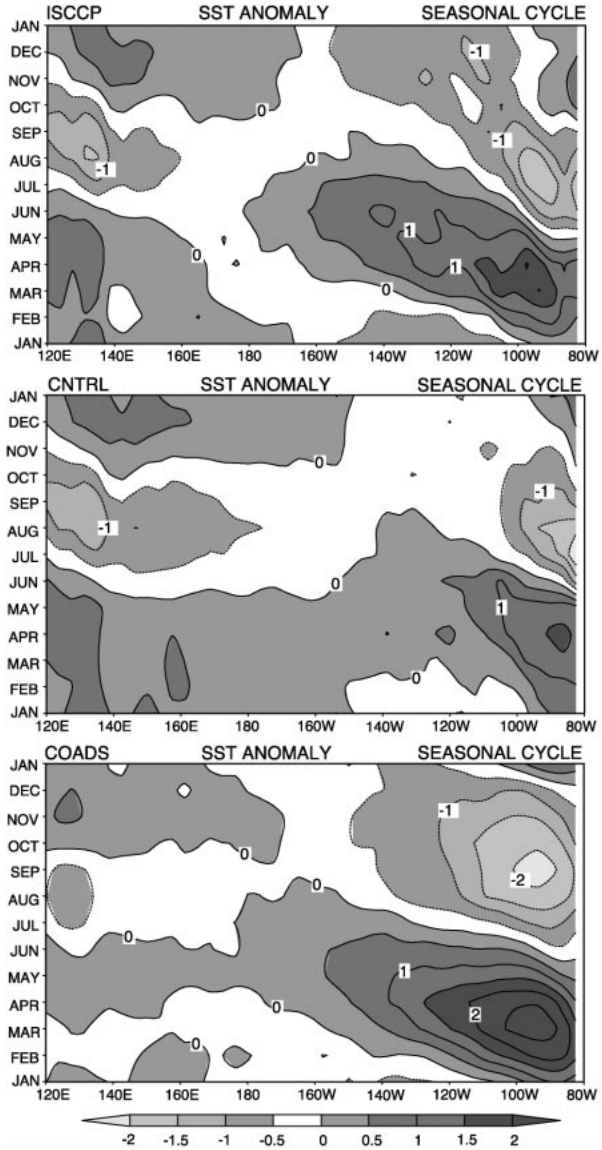

FIG. 7. Longitude–time section (Hovmöller diagram) of SST anomalies with respect to the annual mean climatologies in Fig. 5, at latitude 1.8°S. Longitude = 120°E–80°W; time range = one seasonal cycle. (top) ''ISCCP,'' (middle) CNTRL, and (bottom) COADS. Contour interval = 0.5°C. Progressively darker shading from colder to warmer values, except none for −0.5 to 0°C. Negative contours are dashed.

slight warm bias, while NOLOW exhibits a weak semiannual cycle and a large warm bias in Niño-3.

Essentially only the ''ISCCP'' and COADS SST curves exhibit an annual cycle. In contrast, all four curves of total surface heat flux display a significant semiannual cycle. Thus, the seasonal cycle of total surface heat flux, by itself, cannot adequately explain the seasonal cycle of SST. This is especially true during boreal summer, autumn, and winter, when the dynamical effects are stronger. In early spring, the total surface heat flux, which leads SST by about 1 month in ''ISCCP'' and COADS, has relatively greater impact. The total surface heat flux itself has two main opposing contributions. The first, net shortwave radiative flux (bottom panel) is dominated by a semiannual cycle, in stark contrast to the behavior exhibited farther east by the Niño-1+2 TOA net absorbed shortwave flux (Fig. 3). Conversely, the second, surface latent heat flux, is dominated by an annual cycle, which is somewhat stronger and more realistic in ''ISCCP.''

Of the three simulated total surface heat fluxes in Niño-3, ''ISCCP'' is in best, although imperfect, agreement, in terms of amplitude, with COADS. The largest discrepancy between the four curves occurs during early boreal spring, when low cloudiness in this region should be close to its seasonal minimum value. Then, the ocean receives about 25 W m^{-2} more surface heat flux in ''ISCCP'' than in either CNTRL or NOLOW.

The CNTRL and NOLOW deficits of total surface heat flux during March and April occur for quite different reasons. On one hand, CNTRL receives ~25 W m^{-2} less surface net shortwave flux than either ''ISCCP'' or NOLOW. The reason is that CNTRL predicts too much low cloudiness in Niño-3 during spring (not shown). On the other hand, NOLOW loses nearly 25 W m^{-2} more surface latent heat flux to the atmosphere than either ''ISCCP'' or CNTRL, and virtually lacks an annual cycle. The primary cause of enhanced evaporation in NOLOW must be its strong warm SST bias, since NOLOW has weaker surface wind stresses in Niño-3 than CNTRL or ''ISCCP'' during most of the year.

With regard to the zonal (τ_x) and meridional (τ_y) components of the surface wind stress, all four curves indicate negative values (i.e., easterlies), exclusively, in Niño-3. However, ''ISCCP'' and COADS have stronger easterly surface wind stresses than CNTRL, while the easterlies in NOLOW are even weaker than in CNTRL. None of the four τ_x curves exhibit a well-defined annual cycle, although ''ISCCP'' tends to exhibit slightly weaker easterlies in early spring, about 1 month earlier than COADS and 2 months earlier than CNTRL. Conversely, all four τ_y curves exhibit well-defined annual cycles of comparable amplitude in Niño-3. However, only in ''ISCCP,'' in better agreement with COADS, does a southerly meridional component, and hence a southeasterly surface wind stress prevail year-round in Niño-3. Southeasterly cross-equatorial surface wind stresses are conducive to upwelling through the Ekman drift term, due to the sign change in the coriolis parameter across the equator. Thus, in ''ISCCP,'' the absence of northerlies in spring enhances equatorial upwelling, despite weaker easterlies, at that time. A similar scenario should apply for coastal upwelling in the extreme southeastern tropical Pacific. The intermediate coupled model of Xie (1998) produces a realistic equatorial cold tongue only when external southerly τ_y forcing is turned on, thus emphasizing its importance. Also, Bergman and Hendon (2000) suggest that the atmospheric (i.e., TOA

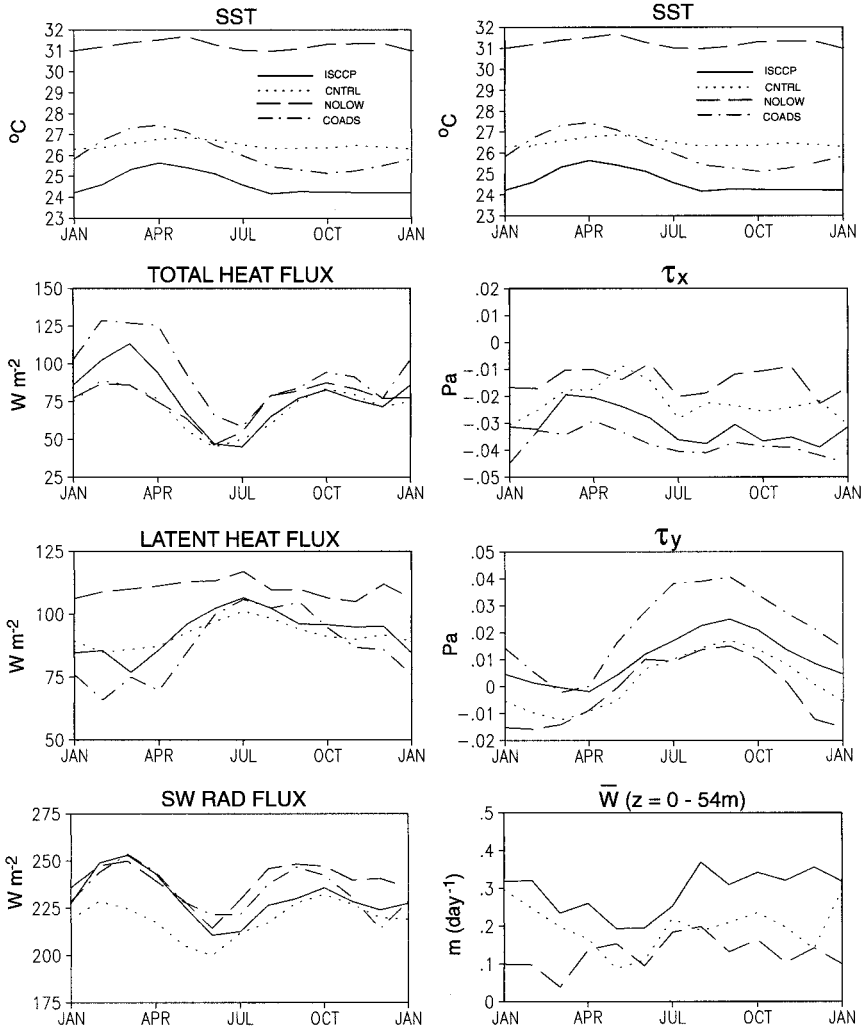

FIG. 8. Time series of Niño-3 (150°–90°W, 5°S–5°N) climatological monthly mean diagnostics for ''ISCCP,'' CNTRL, NOLOW (1985–2004), and COADS (1950–89). Left: (top) SST (°C), (second) total heat flux into the ocean, (third) latent heat flux into the atmosphere, and (bottom) net shortwave radiative flux into the ocean (W m^{-2}). Right: (top) SST (°C), (second) surface wind stress components (second) τ_x and (third) τ_y (Pa), and (bottom) $\overline{w_T}$, the oceanic vertical motion, averaged over the upper 54 m (m day^{-1}).

minus surface) cloud radiative forcing may be indirectly responsible for the seasonal cycle of SST in the cold tongue region, through its impact on the meridional wind component.

The seasonal cycles of monthly mean Niño-3 oceanic vertical velocity, $\overline{w_T}$, averaged from the surface (level 1) to a depth of 54 m (level 6), and τ_x appear to be negatively correlated, consistent with the expected response of upwelling to wind stress. The equatorial upwelling is clearly stronger in ''ISCCP'' than in either CNTRL or NOLOW, and only in ''ISCCP'' does it have a discernible annual harmonic.

Since evaporation is proportional to the surface wind speed, the surface evaporation weakens in ''ISCCP,'' as τ_y approaches 0 (and the surface zonal wind stress, τ_x, relaxes somewhat) during late winter and early spring. Not surprisingly ''ISCCP'' displays a stronger annual cycle in latent surface heat flux (Fig. 8) than CNTRL. Surface latent heat flux tends to lead τ_y by 1–2 months. The simulated seasonal cycles of Niño-3 SST and τ_y are visually correlated, with τ_y leading SST by perhaps 1 month.

In short, our results suggest that MSc cloud forcing in the southeastern tropical Pacific has a nonlocal positive impact upon surface dynamical cooling and surface latent heat flux to the west-northwest, in Niño-3. Both mechanisms contribute to the maintenance of the annual cycle of SST there, whereas locally, shortwave radiative forcing elicits a semiannual response. As Yu and Mechoso (1999) have shown, and as our annual cycle results in

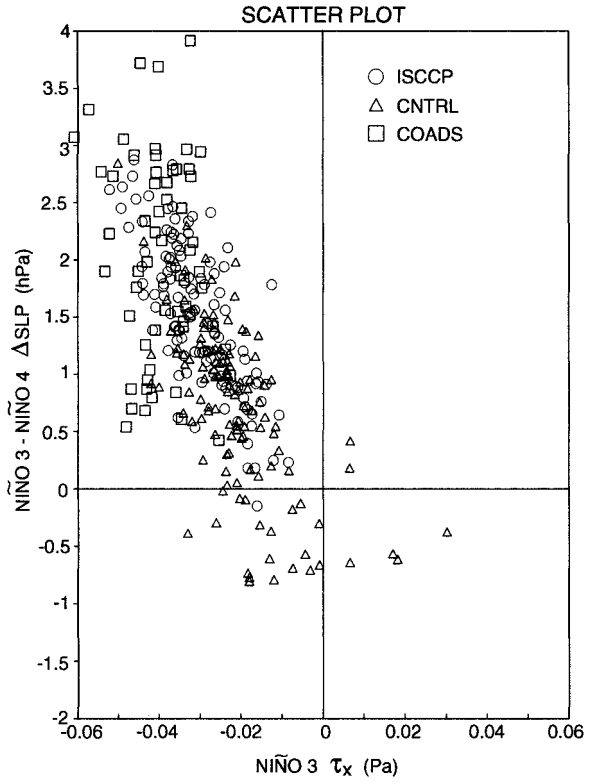

FIG. 9. Scatterplot of Niño-3 minus Niño-4 SLP difference vs Niño-3 zonal surface wind stress τ_x. Each symbol represents one monthly mean during the 10-yr period 1985–94 (''ISCCP'' and CNTRL) or the 8-yr period 1982–89 (COADS).

Niño-3 suggest, the robust annual cycle aspect of the MSc cloud forcing plays a key role. Cloud–dynamical interactions will be discussed further in section 6.

d. Further analysis of tropical surface wind stress and sea level pressure responses

The sea level pressure (SLP) and its relationship to the zonal surface wind stress, τ_x, constitute part of the equatorial dynamical response. The east–west SLP gradient across the central equatorial Pacific (not shown) is more realistic and generally more intense in ''ISCCP'' than in CNTRL. The simulated SLP gradients are weakest around April. Then, as the southeastern subtropical Pacific surface high intensifies and expands, they migrate westward, more or less in synch with the respective seasonal migrations of SST.

The relationship between the east–west SLP gradient and τ_x in the equatorial Pacific is explored in Fig. 9. There, scatter diagrams of contemporaneous simulated and observed Niño-3 minus Niño-4 monthly mean SLP difference Δ_x(SLP) versus Niño-3 monthly mean τ_x are plotted. The Niño-3 and Niño-4 boxes are bounded by 150°–90°W, 5°S–5°N, and 160°E–150°W, 5°S–5°N, respectively. For legibility, only 10 yr (years 4–13) or 120 points are represented.

A rather robust relationship exists between simulated surface zonal wind stress and SLP. In ''ISCCP,'' all but one of the points fall in the upper-left quadrant. For these points, the near-equatorial surface zonal wind stress is easterly, while the near-equatorial sea level pressure increases from west to east across the date line. The highest correlation coefficient (~0.61) associated with the best least squares fit was obtained for ''ISCCP.'' A comparable value was also obtained for ''ISCCP'' monthly mean *anomalies* with respect to the 10-yr mean monthly mean climatology. However, the correlation coefficient was much lower, that is, ~0.35 when the corresponding ''ISCCP'' monthly mean climatologies were regressed. One interpretation is that the timescale for the mutual adjustment of surface wind stress and zonal SLP gradient is relatively short. CNTRL points tend to cluster beneath ''ISCCP'' points, where the SLP gradient is weaker, and to the right, where the Niño-3 easterly wind stress is weaker. In fact, some CNTRL points even fall into the other three quadrants. CNTRL exhibits somewhat more scatter than ''ISCCP.'' Large scatter is associated with weak SLP gradients. Intriguingly, both simulated distributions exhibit a stronger relationship than COADS. The relatively sparse density of observed data may be a contributing factor.

According to Lindzen and Nigam (1987), ''flows forced directly by surface temperature are often comparable to observed low-level flows in both magnitude and distribution.'' Their theory may help to explain the mutual relationships between our simulations of SST, surface zonal wind stress, and SLP gradient in the equatorial Pacific. Recall that the zonal gradient of SST is enhanced in our simulations by specifying quasirealistic MSc clouds. The two leading terms of the atmospheric zonal equation of motion at the surface, that is, $-\rho^{-1}(\partial p/\partial x)$ and $\rho^{-1}\partial\tau_x/\partial z$, are in approximate balance near the equator, since $f \cong 0$. (Here, p = pressure, ρ = density, f = the Coriolis parameter, and z = height.) It is assumed that the (zonal) pressure gradient is confined essentially to the planetary boundary layer of fixed depth. Under those conditions, τ_x should be strongly related to the zonal gradient of SLP.

e. Equatorial subsurface temperature and zonal current responses

Longitude–depth sections of ''ISCCP,'' CNTRL, and NOLOW 20-yr climatological annual mean ocean temperature and zonal current at latitude 0.1°S are displayed in Fig. 10. Clearly, the three simulations generate very different annual mean ocean temperature cross sections. ''ISCCP'' verifies best, overall, against the Levitus (1982) ocean temperature climatology (not shown).

In the western equatorial Pacific, the warm SSTs of NOLOW raise its heat content, whereas CNTRL and especially ''ISCCP'' have progressively colder SSTs and less heat content. In the eastern equatorial Pacific, the depth of the 20°C isotherm, Z_{20C}, varies dramatically.

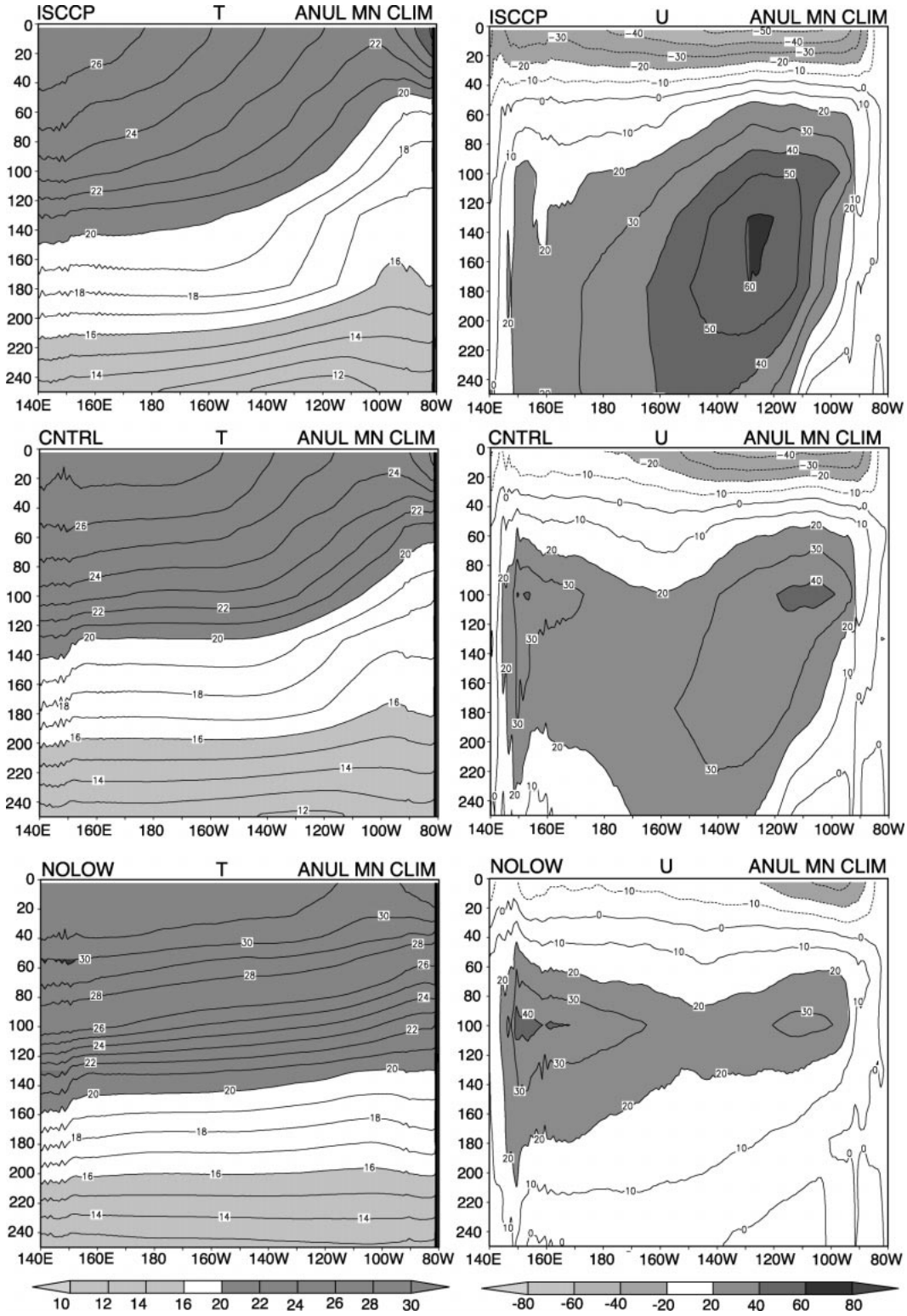

FIG. 10. Longitude–depth sections (140°E to 80°W; 0–250 m) of 20-yr climatological (left) annual mean ocean temperature and (right) zonal current at latitude 0.1°S. (top) ''ISCCP,'' (middle) CNTRL, and (bottom) NOLOW. Temperature contour interval = 1°C. Darker shading >20°C, lighter shading <16°C, and no shading 16°–20°C. Zonal current contour interval = 10 cm s^{-1}. Progressively darker shading from <−20 to >80 cm s^{-1}, except none from −20 to 20 cm s^{-1}. Negative contours are dashed.

The isotherms slope considerably more steeply in ''ISCCP'' than in CNTRL, and over a broader longitudinal domain. The ''ISCCP'' *annual mean* east–west SST difference across the equatorial Pacific is comparable to that in CNTRL, but is not confined east of the date line. During summer into early autumn (not shown), the east–west SST gradient over the eastern equatorial Pacific is significantly stronger in ''ISCCP'' than in CNTRL. In NOLOW, the annual mean isotherms are oriented nearly horizontally, and the east–west SST gradient is extremely weak across the entire equatorial Pacific. The above results are consistent with the seasonal excursion of the ''ISCCP'' equatorial cold tongue and surface winds. Enhanced remote dynamical cooling, triggered by MSc, evidently plays a role, since the ''ISCCP'' minus CNTRL shortwave radiative cooling response is generally confined east of longitude 120°W. Moreover, in spring, the Niño-3 ''ISCCP'' minus CNTRL surface shortwave radiative flux difference is actually positive, corresponding to warming in Niño-3, as CNTRL generates more cloudiness than ''ISCCP'' there.

The *annual mean* cross sections of ocean zonal current at latitude 0.1°S are dynamically consistent with the temperature cross sections. ''ISCCP'' has the strongest (and deepest) south equatorial current (SEC), while CNTRL and NOLOW have progressively weaker ones. Likewise, ''ISCCP'' has a deeper, more intense (westerly) Equatorial Undercurrent (EUC) than CNTRL; and its core lies 20° farther west. In comparison, NOLOW has a very weak and shallow secondary jet core in the eastern Pacific, whereas its primary EUC jet core is centered in the western equatorial Pacific. Seasonally (not shown), the ''ISCCP'' EUC core in the eastern equatorial Pacific weakens by $\sim$10 cm s^{-1} in autumn, but otherwise remains intact. In contrast, the CNTRL EUC becomes shallower in boreal summer and virtually disappears in autumn, when a shallow western branch emerges west of the date line. The western branch of the NOLOW EUC dominates in summer and early autumn, whereas its eastern branch is slightly stronger in winter.

The NOLOW results in Fig. 10 underscore two points. First, without any tropical MSc, the surface trades and SEC, and hence dynamical cooling, weaken substantially relative to CNTRL. In turn, the east–west SST gradient weakens. Second, with no low clouds in the western equatorial Pacific, more shortwave radiation is absorbed at the ocean surface, thereby warming the SST (see section 4a), and the subsurface layers.

Results from HYB (see Table 1) confirm that it is the low clouds in the *eastern* tropical Pacific that have the most impact, by far, on the intensification of the dynamical cooling. East of longitude 120°W, where ISCCP low clouds are specified, as in ''ISCCP,'' the HYB equatorial Pacific SST and zonal surface wind stress responses (not shown) closely resemble those of ''ISCCP.'' Farther west, the HYB SSTs resemble those of NOLOW, though they are not quite as warm, suggesting that enhanced dynamical cooling in the eastern equatorial Pacific has some nonlocal influence. In any case, the essential impact of MSc clouds in the eastern tropical Pacific upon dynamical cooling is not invalidated by either warm or cold SST biases in the west, which arise, locally, in direct response to biases in (net shortwave) surface radiative flux.

5. Multiyear simulations: SST interannual variability response

Monthly mean SST anomalies, that is, departures from the respective monthly mean SST climatologies, have been computed for the last 20 yr of integration (1985–2004) for the ''ISCCP,'' CNTRL, and ISC.8 simulations and for 40 yr (1950–89) of COADS verification data. The former period (like the latter) encompasses several ENSO-like events, yet it excludes most of the spinup period of the three integrations. It is reassuring that the anomaly results from both halves of this 20-yr period are qualitatively similar. The reader is reminded that the specification of monthly mean low cloud fraction in ''ISCCP'' (and ISC.8) is climatological. However, interannually varying low clouds is not a prerequisite for tropical SST interannual variability.

Root mean square (rms) SSTs, calculated from the simulated and COADS SST anomalies, are displayed in Fig. 11. In the southeastern tropical Pacific, adjacent to the west coast of South America, the SST variability exhibited by all three simulations is weaker than observed; and east of the date line, it is substantially more equatorially trapped. Near the equator, ISC.8 exhibits slightly more SST interannual variability than CNTRL, and ''ISCCP'' somewhat less. ISC.8 and especially ''ISCCP'' display longitudinally broader active regions than CNTRL. This aspect tends to compensate for the weaker maximum intensity in ''ISCCP.'' Also, the activity is centered farther west in ''ISCCP'' and ISC.8 than in CNTRL. The stronger equatorial cold tongue in ''ISCCP'' seems to inhibit the eastward progression of warm ENSO-like anomalies east of the date line. For example, in longitude-time sections of simulated monthly mean total SST (or SST anomalies) at latitude 1.8°S (not shown), more warm, ENSO-like events extend all the way across the Pacific in ISC.8 than in ''ISSCP.'' During such events, the MSc cloud forcing, while lacking interannual variability, would likely still be less in error in ISC.8 than in ''ISCCP,'' by virtue of being weaker.

The timescale of simulated SST variability found in the longitude-time sections is characteristic of observed ENSO events. This result is corroborated by a time power spectral analysis (not shown) of monthly mean CNTRL, ''ISCCP,'' and ISC.8 Niño-3 SST indices, that is, Niño-3 box mean SST anomalies. This analysis is based upon a 30-yr record, that is, the simulations were extended 10 yr to enhance the sample size. ISC.8 and

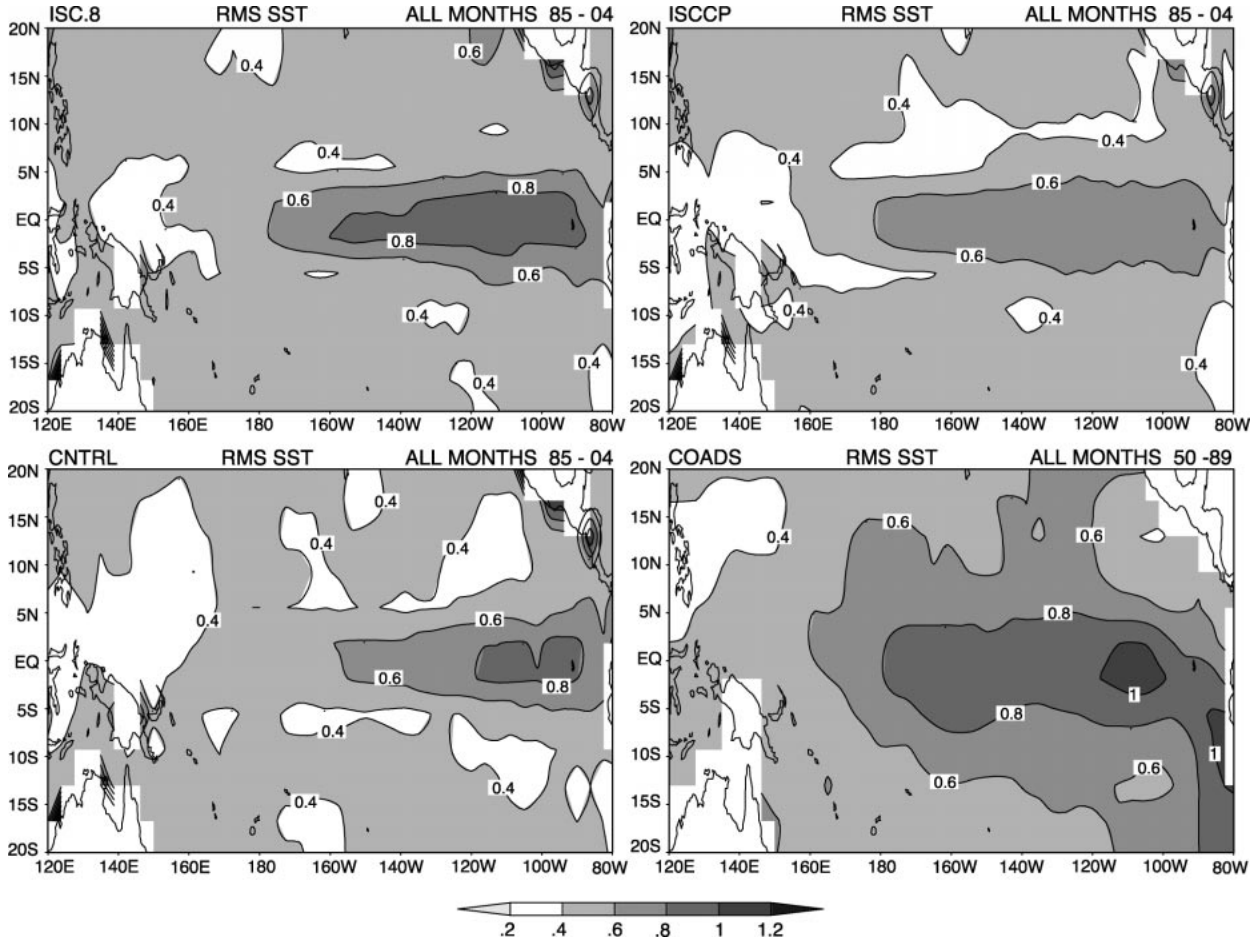

FIG. 11. Contour maps of rms monthly mean SST anomalies over the tropical Pacific basin. (upper left) ISC.8, (upper right) ''ISCCP,'' (lower left) CNTRL, and (lower right) COADS. The rms values are calculated from 20 yr of model integration and 40 yr of COADS analysis. Contour interval = 0.2°C. Progressively darker shading as the rms value increases, except none from 0.2° to 0.4°C. Land is masked (no shading).

CNTRL exhibit three dominant spectral peaks that are quite well aligned. The two peaks near 40 months and near 58 (or 60) months correspond to ENSO. Another peak near 114 months may represent decadal variability. Two ENSO peaks found in ''ISCCP'' near 52 and 70 months are weaker. Moreover, ''ISCCP'' lacks a decadal peak.

Our model's SST variability should be concentrated east of the transition zone between relatively warm and cold equatorial SSTs, where thermocline displacements can interact very effectively with SST. But, strong, climatological MSc cloud forcing could dampen variability, especially in the extreme eastern equatorial Pacific. To see whether our coupled model actually mimics the delayed oscillator mechanism for the ENSO cycle first proposed by Schopf and Suarez (1988), lead–lag correlations between equatorial $\overline{T}^z$ anomalies and Niño-3 SST anomalies are plotted in Fig. 12. Here, $\overline{T}^z$, the temperature averaged over the top 250 m of the ocean, is a proxy for ocean heat content. Lead–lag correlations have been calculated for the ''ISCCP,'' ISC.8, and CNTRL simulations, based upon the last 20 yr of integration, plus an 18-yr MOM ODA, spanning 1980–97. ISC.8 exhibits a robust delayed oscillator response, closely resembling that obtained by Rosati et al. (1997) for their ODA. In both, $\overline{T}^z$ leads Niño-3 SST, with lead increasing from right to left, to about 10 months at longitude 140°E. While CNTRL also resembles a delayed oscillator mode, its response is weaker. In contrast, the orientation of the ''ISCCP'' contours is perhaps more suggestive of a standing SST mode. ''ISCCP'' reveals considerable persistence east of the date line, although the correlation between its $\overline{T}^z$ and Niño-3 SST anomalies is weaker than in ISC.8.

Next, we look for evidence of a seasonally varying coupled ocean–atmosphere instability in our simulations. Tziperman et al. (1998) incorporated a coupled ocean–atmosphere seasonally varying instability strength into a delayed oscillator mechanism for the ENSO cycle. As a result, the onset of El Niño events and the phase of peak anomalies in Niño-3 in their model became essentially phase locked to the seasonal cycle.

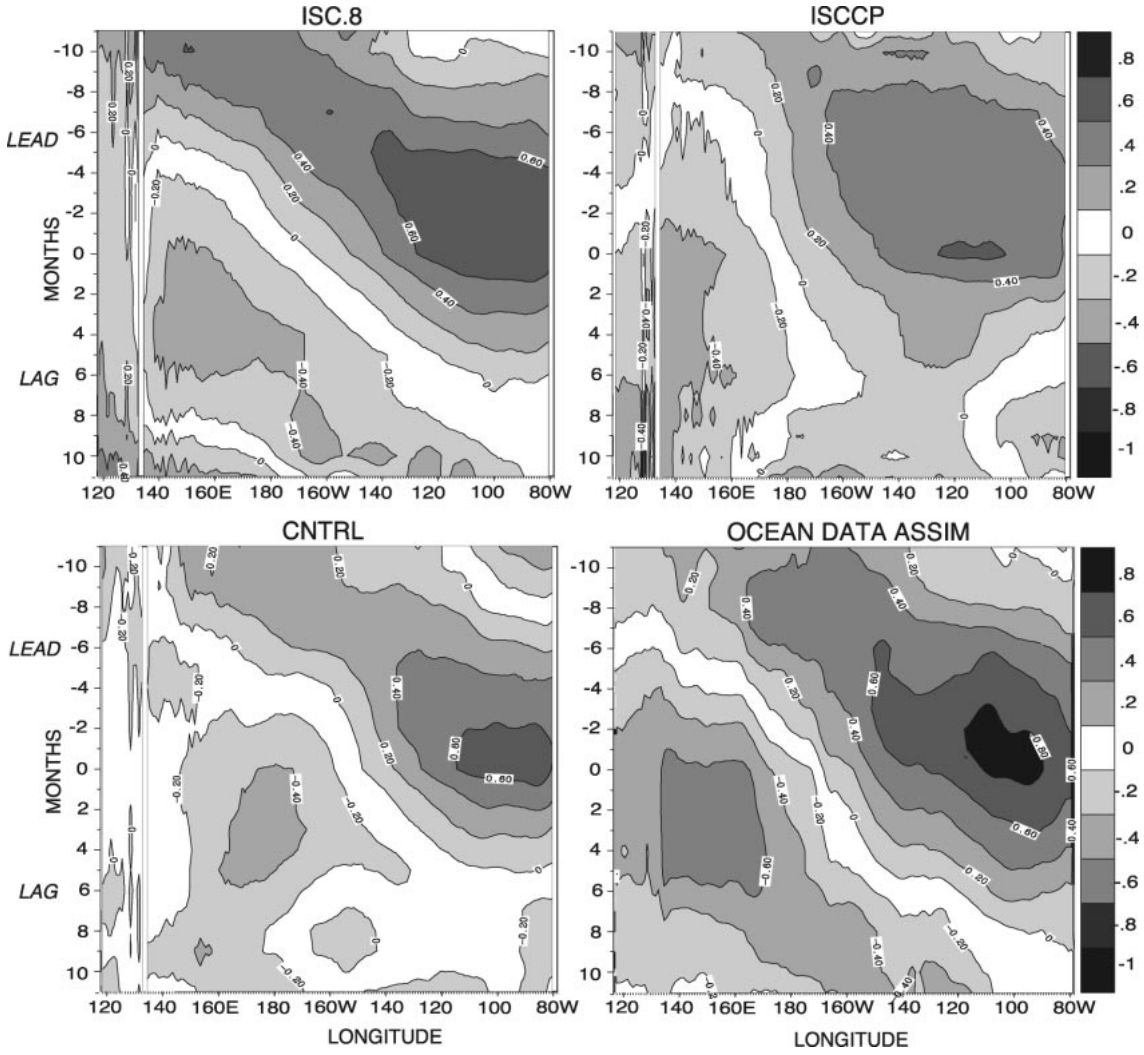

FIG. 12. Lead–lag correlation r of the 5°S to 5°N latitude mean anomaly of ocean temperature $\overline{T}^z$ (vertically averaged over the top 250 m) vs Niño-3 SST anomaly, as a function of longitude (120°E–80°W) and lag (12 to −12 months). Niño-3 SST lags $\overline{T}^z$ where MONTHS <0. (upper left) ISC.8, (upper right) ''ISCCP,'' (lower left) CNTRL, and (lower right) 4D ocean data assimilation. Contour interval = 0.20.

Figure 13 is a longitudinal-time section of rms SST near the equator, based upon contributions from like months only, that is, 20 (or in the case of COADS, 40) Januaries, Aprils, Decembers, etc. It depicts the longitudinal position and amplification of centers of rms SST activity over the equatorial Pacific. The interannual variability is centered near its easternmost position during boreal spring. The springtime peak variability in the eastern equatorial Pacific is strongest in ISC.8 and occurs 1 month earlier in ''ISCCP,'' more in phase with the minimum MSc cloud forcing. For the duration of the year, ''ISCCP'' exhibits weaker variability than the other simulations. With stronger low cloud forcing, its cold SSTs and strong trades become established more rapidly, thereby damping variability. In all simulations, as the action shifts westward during summer and early autumn, its amplitude weakens, then amplifies, again, during middle and late autumn. ''ISCCP'' exhibits the greatest westward shift and CNTRL the least, quite like the seasonal variation of their respective equatorial cold tongues. The peak variability is associated with the mature phase of ENSO-like events. It occurs in ''ISCCP'' and ISC.8 in the east central Pacific in late November, a few weeks earlier than observed. It is most coherent and intense in ISC.8 and weakest in ''ISCCP.'' A second late autumn peak, located farther east, near longitude 110°W, in COADS, is not well simulated. The center of rms SST activity shifts eastward during early spring, in simulations and COADS alike. In many but not all CNTRL and especially ISC.8 robust ENSO events, Niño-3 SST anomalies seem to peak during late fall/early winter, perhaps slightly earlier than the theory of Tziperman et al. (1998) predicts, while the time window for ''ISCCP'' peaks is broader.

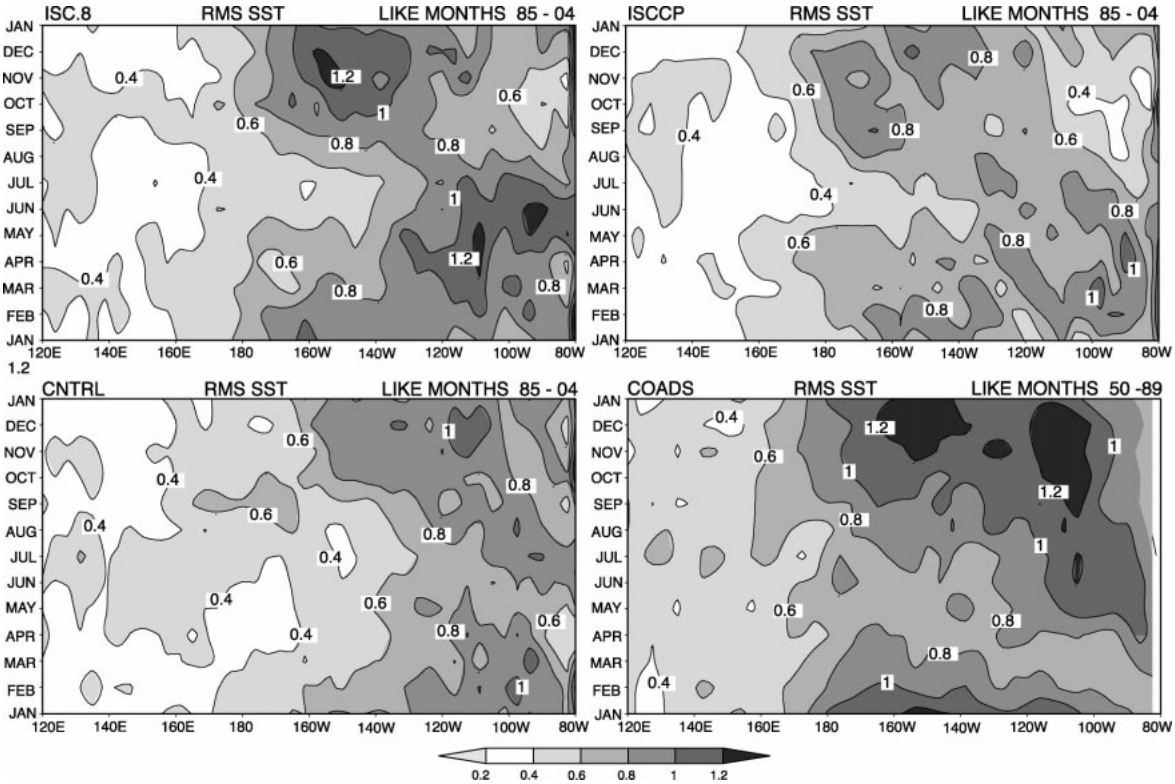

FIG. 13. Longitude–time section (Hovmöller diagram) at latitude 1.8°S of the contribution of like months to the rms monthly mean SST anomalies in Fig. 11. Longitude = 120°–80°W. Time range = one seasonal cycle. Datasets, shading, and contour interval as in Fig. 11.

In short, our coupled model appears to exhibit evidence of three mechanisms associated with the ENSO cycle in the equatorial Pacific. These are: 1) the delayed oscillator, 2) SST variability whose strength (and longitudinal position) is seasonally varying, and 3) phase locking of the onset of El Niño events and the phase of peak anomalies in Niño-3 to the seasonal cycle. However, the above mechanisms appear to be influenced by the MSc cloud forcing. Notably, ''ISCCP'' displays weaker SST interannual variability and delayed oscillator responses than ISC.8 or CNTRL.

Another important finding pertaining to interannual variability is that our coupled system appears to be quite sensitive to a relatively modest 20% relative change in the annual mean and seasonal variation of low cloud fraction. The latter value may be only slightly weaker than the interannual variability of observed Peruvian MSc during boreal summer inferred from Klein and Hartman (1993). Most of the ''ISCCP'' minus ISC.8 differential low cloud forcing is confined to the MSc regions of the southeastern tropical (and secondarily, to the eastern equatorial) Pacific. For example, the absolute differences in ''ISCCP'' minus ISC.8 low cloud fraction in Niño-1+2 and Niño-3 are ~0.16 and ~0.06, respectively, although, the corresponding changes in surface shortwave radiative forcing are nontrivial. Elsewhere in the Tropics, the absolute difference between the ''ISCCP'' and ISC.8 annual mean low cloud fractions tends to be much smaller.

Overall, the ISC.8 simulation may possess the best compromise solution for the seasonal cycle and interannual variability in our coupled model, although not necessarily for the correct reason. Its somewhat weaker MSc cloud forcing (compared to ''ISCCP'') may have less adverse impact upon the eastward progression of warm ENSO-like anomalies. This may help to explain why only ISC.8, and not ''ISCCP'' exhibits a robust delayed oscillator mode response. Nonetheless, it is a bit unsettling, if coupled systems are really so sensitive, as our ''ISCCP'' versus ISC.8 results suggest, to a 20% relative change in the seasonally varying MSc cloud fraction and its annual mean. Indeed, it is quite a challenge to develop a cloud scheme capable of predicting the MSc cloud fraction (and quite possibly low cloud optical depth) in a coupled model, including its seasonal variation and interannual variability, with greater accuracy than 20%!

6. Equatorial cold tongue dynamics

Not only do marine stratocumulus clouds contribute to local radiative cooling in the southeast tropical Pacific, they also enhance dynamical cooling by strengthening the southeast trades and hence coastal and

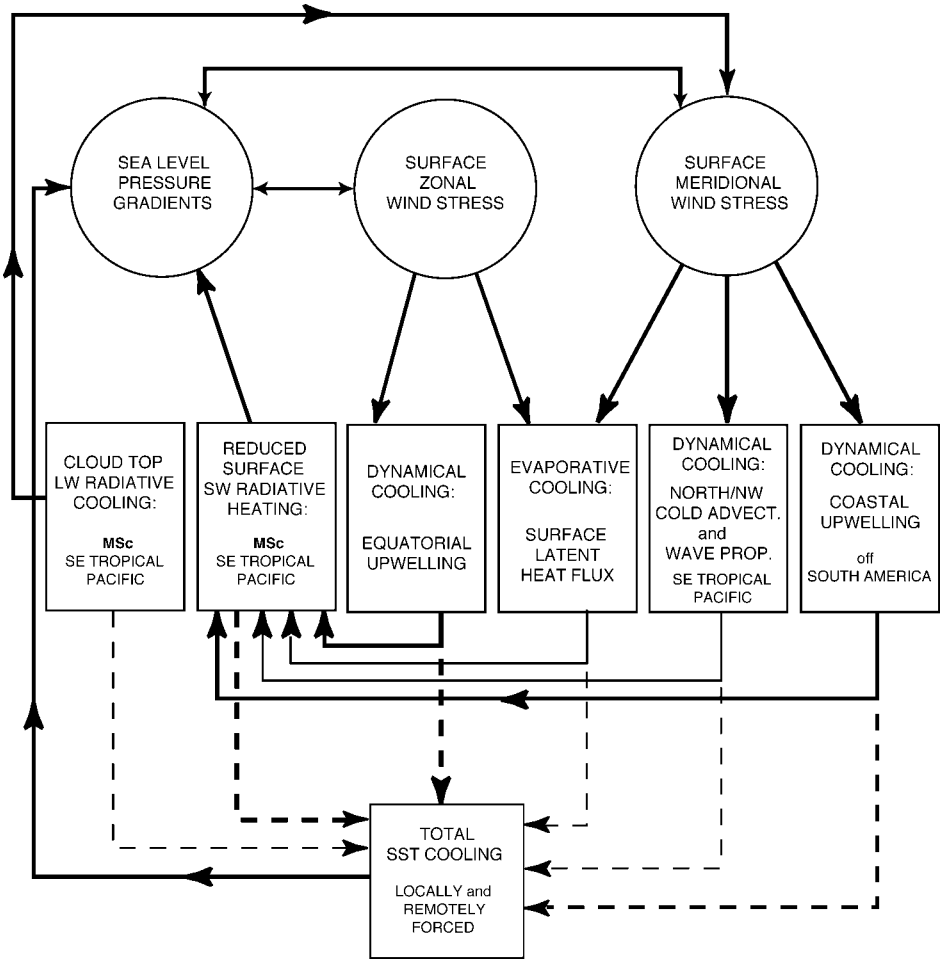

FIG. 14. Flow chart of dynamical and surface heat flux linkages in the southeastern tropical and eastern equatorial Pacific Ocean.

equatorial upwelling, as well as evaporative cooling. The complex suite of potential interactions involved is depicted, schematically, by the flow chart in Fig. 14. The middle row of boxes represent various processes contributing to the total SST cooling in the equatorial Pacific, indicated by the dashed arrows leading to the bottom box and linked to surface dynamical variables, depicted by the circles at the top. Although any of the cooling processes in Fig. 14 could directly affect the surface dynamical variables, only the links from the most important radiative processes associated with MSc clouds, that is, reduced surface insolation and cloud-top longwave radiative cooling, are depicted. Links between the dynamical variables are represented as well. The two arrow thicknesses in the flow chart (subjectively) symbolize the relative strengths of various interactions.

We now apply this conceptual framework to the seasonal cycle of SST. The dynamical feedbacks are qualitatively similar to those proposed by Mitchell and Wallace (1992). However, we focus on their connection to MSc clouds. Around the time of the spring maximum, the southerly meridional surface wind stress near the west coast of South America strengthens along with the (north–south), SLP gradient in the southeast tropical Pacific. Hence, dynamical cooling due to coastal upwelling and evaporative cooling increase. The onset of SST cooling in this region is conducive, locally, to more MSc, and hence to less surface insolation, as well as to more cloud-top longwave radiative cooling (Nigam 1997; Bergman and Hendon 1999). Both radiative processes further strengthen the southerly meridional surface wind stress. In turn the stronger surface southerlies induce locally stronger, more extensive dynamical and evaporative cooling. As stronger southeast trades advect cold water across a sharper gradient, the cool SST region expands to the northwest. Wave propagation may also occur. Northwest expansion of the MSc follows suit, further reinforcing the cooling. In response, the subtropical southeast Pacific high and associated southeasterly trade circulation continue to intensify. This fosters equatorial upwelling and hence equatorial dynamical (as well as evaporative) cooling and westward ex-

pansion of the cold tongue. Reduced surface sensible heat and net longwave radiative flux losses (not shown) should oppose the cooling. Also, colder SSTs should act to diminish the latent heat flux loss caused by the stronger surface trades.

In a *linearized* anomaly model, the contributions of upwelling dynamics, evaporative flux and shortwave radiative flux, associated with MSc clouds, may be summed, as Li and Philander (1996) did. They found that each of these processes contributed to the maintenance of the annual cycle. Moreover, omission of the MSc term did not have catastrophic consequences, because the annual mean surface wind and SST states were specified. In contrast, in a fully coupled model that poorly simulates the seasonal cycle of MSc clouds, the evaporative flux and upwelling dynamical terms may have insufficient strength to sustain the annual cycle of SST in the eastern equatorial Pacific. Thus, the impact of MSc clouds upon dynamical cooling assumes an important role in maintaining the seasonal cycle in our fully coupled nonlinear model.

Li and Philander (1996) maintain that the existence of southerlies and an asymmetric distribution of SST in the far eastern equatorial Pacific throughout the year are crucial for maintaining an annual cycle in the eastern equatorial Pacific. According to this view, a coupled model should be more capable of simulating the seasonal cycle, to the extent that it can achieve those requirements. Indeed, annual mean corrections to the SST and the surface wind fields (Li and Hogan 1999) or to the three-dimensional ocean temperature field (Yang and Anderson 2000) yield improved simulations of the seasonal cycle. Conversely, any fully nonlinear coupled GCM capable of accurately simulating the annual cycle, could hopefully simulate the annual mean state in the eastern equatorial Pacific.

In principle, the mechanisms discussed in conjunction with Fig. 14 should operate on anomalies as well as on the seasonal cycle. In nature, the dynamics modulates the seasonally varying MSc cloud fraction during anomalous warm or cold ENSO-like events. In turn, interannual variations in MSc help to maintain or even reinforce the SST anomalies (Klein and Hartmann 1993). Thus, a true positive feedback loop involving SSTs and MSc clouds is at work. Unfortunately, the ''SST to marine stratocumulus'' link of this positive feedback loop is missing in ''ISCCP,'' since the climatological, seasonally varying low cloud fraction is specified. Essentially, the low cloud–dynamical interaction operates freely in only one direction (cloud to dynamics). Of course, anomalous SSTs and surface winds may still affect sensible and latent heat fluxes and/or produce secondary radiative feedbacks through changes in middle or high cloud fraction.

Clearly, ENSO-like events still occur in our ''ISCCP'' and ISC.8 simulations, even without interannually varying MSc clouds, suggesting that other factors are more important. The latter may include the interannually varying predicted middle and high clouds. Nonetheless, neglecting the interannual variation of MSc clouds could have some adverse impact upon model-simulated ENSO events. MSc cloud forcing should relax during El Niño events and, conversely, strengthen during La Niña events. For example, weaker MSc forcing should favor weaker trades, and hence warmer SST anomalies, locally, off the coast of Peru in spring, and enhanced eastward progression of ENSO-like warm SST anomalies across the Pacific.

7. Concluding remarks

Multiyear simulations have been performed with a fully coupled ocean–atmosphere GCM to examine its tropical sensitivity to a specific model deficiency, that is, the treatment of tropical MSc clouds. The annual mean and annual cycle of the low cloud fraction are both severely underpredicted in the southeastern tropical Pacific in our control run, CNTRL. In contrast, a quasi-realistic MSc cloud regime with improved surface net shortwave radiative flux is achieved in ''ISCCP,'' by specifying ISCCP C2 monthly mean low cloud data.

The simulated annual cycle of SST in the eastern equatorial Pacific is favorably enhanced by quasi-realistic MSc clouds, although a cold bias develops in the Niño-3 region. In the annual mean, the equatorial cold tongue intensifies and the thermocline steepens, while the SST distribution in the eastern tropical Pacific becomes more asymmetric about the equator. Similarly, the annual cycle of SST in the eastern equatorial Pacific becomes more in phase with the seasonal cycle in the southeastern tropical Pacific.

Enhanced dynamical cooling is induced both locally and remotely by the quasi-realistic low clouds (including their *seasonal variation*) in the MSc region. Moreover, the MSc cloud-induced dynamical cooling plays an important role in maintaining the asymmetric distribution of SST about the equator and the annual cycle of SST in the eastern equatorial Pacific. Northerly surface wind stresses are inhibited in the eastern equatorial Pacific in boreal spring, while southerly surface wind stresses and upwelling intensify off the west coast of South America, after the SST maximum occurs. In turn, the annual cycle of surface wind speed and hence surface evaporation strengthens in the southeastern tropical Pacific. Farther west along the equator, the zonal surface wind stress, equatorial upwelling, and the east–west equatorial SST gradient intensify. Beneath the ocean surface, the EUC intensifies, consistent with the steepening of the thermocline. In contrast, all of the above features weaken when there are no low clouds. Although discrepancies between ''ISCCP'' and the observed annual mean climate remain in the tropical Pacific, the surface and subsurface tropical thermal and dynamical responses to quasi-realistic MSc clouds are quite robust.

Interannual variability responds to quasi-realistic MSc clouds as well. The westward extension of the cold

tongue in ''ISCCP'' relative to CNTRL inhibits the eastward progression of its ENSO-like warm events east of the date line. The interannual variability shifts westward with the seasonal excursion of the cold tongue. The *seasonally varying* ''ISCCP'' low cloud fraction over the open ocean is reduced by 20% (i.e., by ≤ 0.16, even in the MSc region) in ISC.8. Given a more relaxed seasonal cycle, ISC.8 exhibits significantly stronger interannual variability than ''ISCCP'' and displays a stronger simulated delayed oscillator response. Also, ISC.8, CNTRL, and, to a lesser extent, "ISCCP" show some inclination for phase locking to the annual cycle. The lack of two-way cloud–dynamical interactions (which would occur if interannually varying MSc clouds could be well predicted), may have weakened our ''ISCCP'' and ISC.8 El Niño and La Niña events somewhat. In any case, the apparent sensitivity of the interannual variability response to a modest 20% reduction in ISCCP MSc cloud fraction makes the dual objectives of accurately forecasting ENSO events while maintaining a realistic zonal SST gradient and annual cycle in the east much more challenging.

Although the impact of MSc has been our primary focus, our coupled model also exhibits a strong SST sensitivity in the western tropical Pacific to the removal of low clouds. There, the SST warms $\sim$5.5°C, transforming an $\sim$2.5°C cold bias in ''ISCCP'' into a 3°C warm bias in NOLOW. Roughly 4.5°C of the warming is attributed to a local decrease in low cloud fraction (from 25%–30% to 0%) and a corresponding $\sim$66 W m^{-2} increase in surface net shortwave radiation. Our low cloud optical depth is apparently excessive in the western tropical Pacific. Thus, coupled modelers should note that SST in the warm pool region may be quite sensitive to errors in either (low) cloud fraction or cloud optical depth.

By isolating and correcting for a specific model deficiency (instead of applying an omnibus flux adjustment), this approach has aided our own coupled model development. As an outgrowth of the present study, we plan to examine the impact of quasi-realistic MSc clouds and low clouds in the western tropical Pacific on *seasonal ENSO forecasts* by a fully coupled GCM. First, in addition to specifying the low cloud fraction, low cloud optical depth over the open ocean will be derived from ISCCP D2 data. The objective is to reduce the model's current low cloud optical depth and shortwave radiative flux biases in the western and central tropical Pacific. In turn, the SST cold bias there should decrease, based upon its sensitivity to ''ISCCP'' versus NOLOW low cloud fraction in the current model. Specification of ISCCP-derived low cloud optical depths is intended as an interim fix, until a prognostic cloud water scheme, which produces a realistic spatial distribution of cloud optical depths, can be developed. Second, a scheme to predict tropical MSc cloud fraction anomalies about the ''ISCCP'' seasonally varying climatological mean is being developed. The scheme permits two-way MSc cloud–dynamical interactions. The hope is that the predicted MSc cloud fraction anomalies will vary significantly between El Niño and La Niña events, thereby improving the seasonal ENSO prediction.

Acknowledgments. We deeply appreciate the many valuable suggestions and comments on the manuscript offered by Anthony Broccoli, Stephen Klein, and Jerry Mahlman of the Geophysical Fluids Dynamics Laboratory, and by Anthony Slingo and an anonymous reviewer. Catherine Raphael and Jeffrey Varanyak edited the computer-generated figures with great enthusiasm and skill.

REFERENCES

Barkstrom, B. R., E. F. Harrison, and R. B. Lee III, 1990: Earth Radiation Budget Experiment, preliminary seasonal results. *Eos, Trans. Amer. Geophys. Union,* **71,** 297, 304–305.

Bergman, J. W., and H. H. Hendon, 2000: The impact of clouds on the seasonal cycle of radiative heating over the Pacific. *J. Atmos. Sci.,* **57,** 545–566.

Browning, K. A., 1994: Survey of perceived priority issues in the parameterizations of cloud-related processes. *Quart. J. Roy. Meteor. Soc.,* **120,** 483–487.

Cess, R., and Coauthors, 1994: Absorption of solar radiation by clouds: Observations versus models. *Science,* **267,** 496–499.

Chang, P., 1996: The role of the dynamic ocean–atmosphere interactions in the tropical seasonal cycle. *J. Climate,* **9,** 2973–2985.

da Silva, A. M., C. C. Young, and S. Levitus, 1994: *Atlas of Surface Marine Data 1994.* Vol. 1, *Algorithms and Procedures,* U.S. Department of Commerce, NOAA, NESDIS, 83 pp.

Gordon, C. T., 1992: Comparison of 30-day integrations with and without cloud-radiation interaction. *Mon. Wea. Rev.,* **120,** 1244–1277.

——, and W. F. Stern, 1982: A description of the GFDL global spectral model. *Mon. Wea. Rev.,* **110,** 625–644.

Horel, J. D., 1982: On the annual cycle of the tropical Pacific atmosphere and ocean. *Mon. Wea. Rev.,* **110,** 1863–1878.

Klein, S. A., and D. L. Hartmann, 1993: The seasonal cycle of low stratiform clouds. *J. Climate,* **6,** 1587–1606.

Levitus, S., 1982: *Climatological Atlas of the World Ocean.* U.S. Govt. Printing Office, 173 pp.

Li, T., and G. Philander, 1996: On the annual cycle of the eastern equatorial Pacific. *J. Climate,* **9,** 2986–2998.

——, and T. F. Hogan, 1999: The role of the annual mean climate on seasonal and interannual variability in a coupled GCM. *J. Climate,* **12,** 780–792.

Lindzen, R. S., and S. Nigam, 1987: On the role of sea surface temperature gradients in forcing low-level winds and convergence in the Tropics. *J. Atmos. Sci.,* **44,** 2418–2436.

Ma, C.-C., C. R. Mechoso, A. W. Robertson, and A. Arakawa, 1996: Peruvian stratus clouds and the tropical Pacific circulation: A coupled ocean–atmosphere GCM study. *J. Climate,* **9,** 1635–1645.

Mechoso, C. R., and Coauthors, 1995: The seasonal cycle over the tropical Pacific in coupled ocean–atmosphere general circulation models. *Mon. Wea. Rev.,* **123,** 2825–2838.

Mitchell, T. P., and J. M. Wallace, 1992: The annual cycle in equatorial convection and sea surface temperature. *J. Climate,* **5,** 1140–1156.

Neelin, J. D., and Coauthors, 1992: Tropical air–sea interaction in general circulation models. *Climate Dyn.,* **7,** 73–104.

Nigam, S., 1997: The annual warm to cold phase transition in the eastern equatorial Pacific: Diagnosis of the role of stratus cloud, top cooling. *J. Climate,* **10,** 2447–2467.

——, and Y. Chao, 1996: Evolution dynamics of tropical ocean–atmosphere annual cycle variability. *J. Climate,* **9,** 3187–3205.

Pacanowski, R. C., 1995: MOM 2 documentation user's guide and reference manual. GFDL Ocean Tech. Rep. 3, GFDL/NOAA, 232 pp. [Available from GFDL/NOAA, P.O. Box 308, Princeton, NJ 08542-0308.]

Philander, S. G. H., D. Gu, D. Halpern, G. Lambert, N. C. Lau, T. Li, and R. C. Pacanowski, 1996: Why the ITCZ is mostly north of the equator. *J. Climate,* **9,** 2958–2972.

Pinker, R. T., and I. Laszlo, 1992: Modeling surface solar irradiance for satellite applications on a global scale. *J. Appl. Meteor.,* **31,** 194–211.

Rayner, N. A., E. B. Horton, D. E. Parker, C. K. Folland, and R. B. Hackett, 1996: Version 2.2 of the global sea-ice and sea surface temperature data set, 1903–1994. UKMO Clim. Res. Tech. Note 74, 21 pp. [Available from Hadley Centre for Climate Prediction Research, U.K. Meteorological Office, London Rd., Bracknell, Berkshire RG12 2SY, United Kingdom.]

Rosati, A., R. Gudgel, and K. Miyakoda, 1995: Decadal analysis produced from an ocean data assimilation system. *Mon. Wea. Rev.,* **123,** 2206–2228.

——, K. Miyakoda, and R. Gudgel, 1997: The impact of ocean initial conditions on ENSO forecasting with a coupled model. *Mon. Wea. Rev.,* **125,** 754–772.

Rossow, W. B., and R. A. Schiffer, 1991: ISCCP cloud data products. *Bull. Amer. Meteor. Soc.,* **72,** 2–20.

Schopf, P. S., and M. J. Suarez, 1988: Vacillations in a coupled ocean–atmosphere model. *J. Atmos. Sci.,* **45,** 549–566.

Seager, R., and R. Murtugudde, 1997: Ocean dynamics, thermocline adjustment, and regulation of tropical SST. *J. Climate,* **10,** 521–534.

Sirutis, J., and K. Miyakoda, 1990: Subgrid scale physics in 1-month forecasts. Part 1: Experiment with four parameterization packages. *Mon. Wea. Rev.,* **118,** 1043–1064.

——, and A. Rosati, 1996: The impact of cumulus convection parameterization in coupled air–sea models. Preprints, *11th Conf. on Numerical Weather Prediction,* Norfolk, VA, Amer. Meteor. Soc., 348–350.

Slingo, J. M., 1987: The development and verification of a cloud prediction scheme for the ECMWF model. *Quart. J. Roy. Meteor. Soc.,* **113,** 899–927.

Stern, W., and K. Miyakoda, 1995: Feasibility of seasonal forecasts inferred from multiple GCM simulations. *J. Climate,* **8,** 1071–1085.

Tziperman, E., M. A. Cane, S. E. Zebiak, Y. Xue, and B. Blumenthal, 1998: On the locking of El Niño's peak time to the end of the calendar year in the delayed oscillator picture of ENSO. *J. Climate,* **11,** 2191–2199.

Wallace, J. M., T. P. Mitchell, and C. Deser, 1989: The influence of sea-surface temperature on surface wind in the eastern equatorial Pacific: Seasonal and interannual variability. *J. Climate,* **2,** 1492–1499.

Wang, B., 1994: On the annual cycle in the tropical eastern central Pacific. *J. Climate,* **7,** 1926–1942.

Xie, S.-P., 1996: Westward propagation of latitudinal asymmetry in a coupled ocean–atmosphere model. *J. Atmos. Sci.,* **53,** 3236–3250.

——, 1998: Ocean–atmosphere interaction in the making of the Walker circulation and equatorial cold tongue. *J. Climate,* **11,** 189–201.

Yang, X.-Q., and J. L. Anderson, 2000: Correction of systematic errors in coupled GCM forecasts. *J. Climate,* **13,** 2072–2085.

Yu, J.-Y., and C. R. Mechoso, 1999: Links between annual variations of Peruvian stratocumulus clouds and of SST in the eastern equatorial Pacific. *J. Climate,* **12,** 3305–3318.